Utilization of Superheated Geothermal Fluid

by

Steindór Hjartarson

Thesis

Master of Science in Sustainable Energy Engineering

January 2012

Utilization of Superheated Geothermal Fluid

Steindór Hjartarson

Thesis submitted to the School of Science and Engineering at Reykjavík University in partial fulfillment of the requirements for the degree of

Master of Science in Sustainable Energy Engineering

January 2012

Thesis Committee

Dr. Guðrún Sævarsdóttir, Reykjavik University, Iceland - Supervisor
Dr. Halldór Pálsson, University of Iceland, Iceland
Kristinn Ingason, Mannvit Engineering, Iceland
Dr. William S. Harvey, Reykjavik University, Iceland

Examiner

Geir Þórólfsson

To my beautiful wife

Utilization of Supercritical Geothermal Fluid

Abstract

Volatile chloride (HCl) is found in geothermal fluids all over the world. When dry steam containing HCl cools to acid dew point, the compound dissolves in the condensate and forms hydrochloric acid. This can have tremendous consequences for piping and equipment as hydrochloric acid aggressively attacks steel and other metals. Severe pitting corrosion can occur and, if this happens in the turbine, cracks can form at the bottom of the pits, which will grow larger with fatigue corrosion and lead to a stress corrosion cracking. The Icelandic Deep Drilling Project (IDDP) is dealing with extreme circumstances with high enthalpy, superheated geothermal steam containing HCl. Successful corrosion mitigation is essential for the feasibility of the development of this promising recource. There are several possible methods for removing HCl from geothermal steam and the goal of this work is to map the applicability of each steam scrubbing technology, taking into account exergy conservation and cost.

Keywords: superheated steam, corrosion mitigation, volatile chloride, wet scrubbing, dry scrubbing, IDDP

Nýting á yfirhitaðri jarðgufu

Útdráttur

Vetnisklóríð (HCl) er að finna í jarðhitagufu um allan heim. Þegar þurr gufa sem inniheldur HCl kólnar niður að daggarmörkum, leysist sameindin upp í þéttivatninu og myndar saltsýru. Þetta getur haft slæmar afleiðingar fyrir leiðslur og búnað, þar sem saltsýra getur valdið holutæringu í stáli og öðrum málmum. Ef þetta gerist í hverflum, geta sprungur myndast neðst í holunum, sem vaxa með þreytutæringu og geta leitt spennutæringar. Íslenska djúpborunarverkefnið (IDDP) er að glíma við yfirhitaða gufu með háu vermi sem inniheldur HCl. Hagkvæmni IDDP byggir að hluta til á árangri aðferða við að draga úr tæringu. Það eru nokkrar mögulegar aðferðir til að fjarlægja HCl úr jarðhitagufu og er markmið þessarar vinnu er að kortleggja notagildi hverrar hreinsunaraðferðar, með tilliti til kostnaðar og varðveislu á exergíu.

Lykilorð: yfirhituð gufa, tæringarvörn, vetnisklóríð, vothreinsun, þurrhreinsun, IDDP

Utilization of Supercritical Geothermal Fluid

Steindór Hjartarson

Thesis submitted to the School of Science and Engineering at Reykjavík University in partial fulfillment of the requirements for the degree of
Master of Science in Sustainable Energy Engineering

Student

_____

Steindór Hjartarson

Supervisor

_____

Guðrún Sævarsdóttir

Acknowledgements

I owe my deepest gratitude to dr. Guðrún Sævarsdóttir, who has provided advice, guidance, and support from the beginning to the end, in numerous ways. I am also grateful for all the time and advice given by Kristinn Ingason, Bjarni Pálsson, William S. Harvey, and Halldór Pálsson.

I am deeply thankful for the financial support of the Geothermal Research Group, Georg. This product would never have come to pass without it.

I also want to thank Mannvit Engineering and Landsvirkjun for data and hands-on experience at IDDP-1, Sveinbjörn Hólmgeirsson and Sigurður H. Markússon for their input to this study, and the Library and Information Services at Reykjavik University.

At last I owe my gratitude to my wife, Dagný B. Stefánsdóttir for her endless support, and to all my family and friends who have stood by me.

Contents

List of Figures

List of Tables

Nomencalture

A	Area [m^2]
E	Exergy [kJ]
h	Enthalpy [kJ/kg]
h	Heat transfer coefficient [$W/m^2\ ^\circ C$]
H	Height [m]
$\dot{m}$	Mass flow rate [kg/s]
p	Pressure [bar]
Q	Heat transfer [kJ]
r	Radius [m]
s	Entropy [kJ/kgK]
T	Temperature [$^\circ C$]
U	Overall heat transfer coefficient [$W/m^2\ ^\circ C$]
W	Work [kJ]
x	Steam quality
η	Efficiency
ω	[$g_{\text{water vapor}}/kg_{\text{dry air}}$]

1 Introduction

The rapidly increasing emissions of greenhouse gases from the conversion of fossil fuels to electrical power and utilization for district heating calls for cleaner energy sources. Geothermal energy has become an economic and reliable energy source over the past few decades, due to technical improvements and higher electricity prices. Although the scientific community is presently split in half regarding whether geothermal energy is sustainable or not, everyone agrees that it is more feasible than fossil fuels, with regard to the environment.

Geothermal heat is the governing thermal energy source in Iceland. Iceland is situated on a mid-ocean ridge with abundant volcanic activity. There are several areas in Iceland that are categorized as high-temperature fields and many of them are already being exploited. These fields currently provide steam for seven geothermal power plants with a total installed power capacity of 575MW$_e$ [16].

Corrosion, erosion, and scale formation are the main operational problems in geothermal power plants using high enthalpy fluids. These difficulties differ from one geothermal field to the other, or even from one borehole to the other within the same field. The characteristic of the problem depends on the chemical composition of the geofluid at each time. Hydrogen chloride is an especially problematic compound that can cause severe pitting corrosion when it dissolves in water. If this happens in a turbine, cracks can form at the bottom of the pits, which will grow larger with fatigue corrosion and lead to a final breakdown with stress corrosion cracking.

There are methods available to remove the harmful substances and prevent such damage. The most widely used is called wet scrubbing (WS). Other methods are also under development and gaining attention, such as dry steam scrubbing (DSS). Binary cycles have also been introduced to the discussion in this context. The cycle does not actually prevent corrosion for it may take place in the heat exchanger instead of the turbine, but that is easier to handle. Little work has been done in comparing the methods' applicability with respect to exergy conservation and cost. That is, how well do the different methods prevent corrosion, how much exergy is lost during the process, and is it cost efficient?

The Icelandic Deep Drilling Project (IDDP) has the main goal of finding out if it is economically and technically feasible to extract supercritical fluids from hydrothermal systems. The intention is to access fluid at supercritical conditions and bring it to the surface as superheated steam ($600-800^{\circ}$C) at subcritical pressure (<220bar) [5]. One attempt has been made to drill such a borehole, that ended in a magma intrusion at 2104m depth [22]. The shallow depth entails downhole pressure of around 120bar, but a flowtest measured enthalpy of around 3100kJ/kg [12]. This well, IDDP-1, contains volatile chloride and other contaminants that re-

quire the geofluid to undergo special treatment before utilization.

An identified need of the IDDP that has not been extensively explored is to assess the various power conversion or fluid utilization options possible for the geofluid once it has been brought above ground. This study is intended to find the possible utilization methods and compare them with respect to power production.

1.1 Structure of the Thesis

At the beginning of this study, in section 2, the reader is introduced to fundamental concepts of power cycles, corrosion, and corrosion mitigation. It is important for the reader to be familiar with these concepts for they are referred to later on. The IDDP is also introduced in more detail so that the reader will fully understand its potential advantage.

Following is a more detailed description of the goals of this study, in section 3. The reader is introduced to the combination of power cycles and corrosion mitigation methods that are to be examined with software models, and how their comparison will be carried out. This is accompanied with the design criteria of each model and its corresponding equations.

Next up, in section 4, the raw results from the models are presented to the reader. This includes gross and net power production, condenser duty, exergy destruction in different components, and of course the most important thing, exergy efficiency of each corrosion mitigation method.

Section 5 compares and comments on the results of each model. Also, the benefits of drilling down to depths greater than 3km for geofluids at supercritical conditions will be examined.

At last there is a simple conclusion and comments on future work, as well as appendices and references.

2 Background

2.1 Thermodynamic Power Cycles

It is important for the reader to be familiar with the different thermodynamic power cycles, or simply power cycles, that will be referred to in order to fully understand the study.

A power cycle is a series of thermodynamical processes that affect the properties of a fluid. There are several different power cycles that are used in the geothermal industry, each with their own best applicability. The expected extreme circumstances of the IDDP may require power cycles that are not conventional for a geothermal power plant, and better yet, the extreme circumstances could make for power cycles that to date have only existed in theory, to suddenly become practical. Later on, these different power cycles will be referred to paired with different corrosion mitigation methods.

2.1.1 Dry Steam Cycle

Power plants with a dry steam power cycle have a simple setup and require the smallest amount of equipment of all conventional power cycles used in the geothermal industry. This type of power plant can be used if the fluid at the wellhead is of perfect quality, that is, it contains no liquid. An ideal superheated geofluid could pass directly through a turbine after going through a rock catcher without any additional equipment. After that the steam is condensed to liquid phase before it leaves the power plant. A simple dry steam cycle is shown in Figure 1.

Today, dry steam power plants account for 12% of all geothermal power plants in the world, and 26% of the total installed geothermal capacity [21].

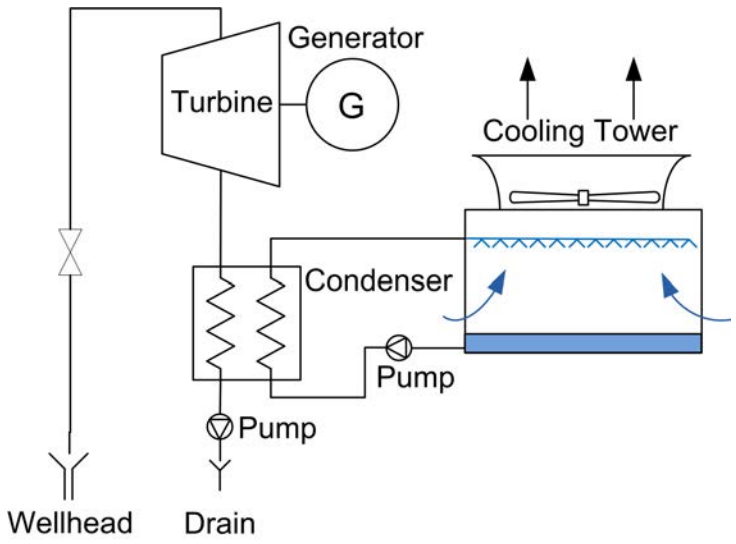

Figure 1: Process diagram of a simple dry steam power cycle.

2.1.2 Single-Flash Cycle

Power plants with a single-flash power cycle account for 42% of the total installed geothermal power capacity in the world [21]. This is frequently the first type installed at a newly developed site for it is relatively simple and cheap to install and operate, and can easily be developed to a more complex power plant. A typical 30MW single-flash power plant needs about 6 production wells producing a mixture of saturated steam and liquid [21]. The two-phase flow is directed to the power plant in pipelines. Before entering the power plant the flow goes through a separator where the phases are parted from each other. The liquid phase leaves the power plant from there, while the steam continues on its way towards the turbine. After that the steam is cooled down to a liquid phase and leaves the power plant. A simple single-flash cycle is shown in Figure 2.

Before the fluid is extracted from the ground through the production wells it is all in a liquid phase due to high pressure. It is referred to as *flashing* when the liquid evaporates, turning into two-phases, due to pressure drop. This can happen in the reservoir, in the production well or in the gathering equipment. As the name implies, in a single flash power plant the fluid is flashed only once.

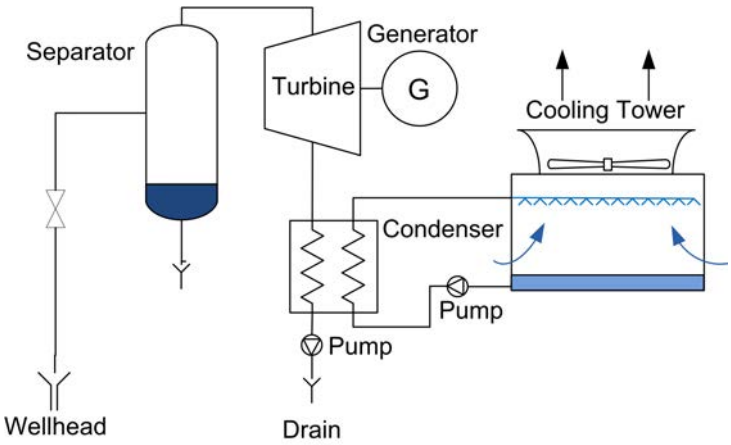

Figure 2: Process diagram of a simple single-flash power cycle.

2.1.3 Binary Cycle

Binary power cycle is often referred to as a *closed power cycle*, while single-flash is an *open power cycle*. In a power plant with a closed cycle, the geofluid never goes through the turbine. The fluid is often kept under pressure so that it doesn't flash, but this type of power plant can also be implemented in a way that the geothermal steam condenses in a heat exchanger. The geofluid flows through a heat exchanger which heats up a working fluid before leaving the power plant. The *Working fluid* flows in a closed cycle; it is heated up in a heat exchanger and

evaporates, drives the turbine, is cooled until it is saturated liquid, and is then heated up again in the heat exchanger. A simple binary cycle is shown in Figure 3.

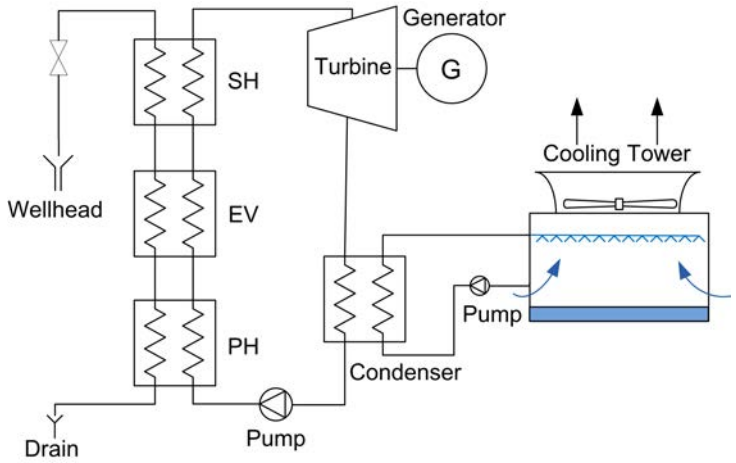

Figure 3: Process diagram of a simple binary power cycle.

Binary power cycles are often used when the temperature of the geofluid is too low for the flash power plants to be efficient, due to technical constraints (below $\sim 180°C$). Working fluids can be selected that evaporate at lower a temperature than water. Also, if the geofluid contains contaminants that can cause considerable corrosion, erosion, or scaling to the turbine, it may be convenient to use a binary power cycle to control the location of the scaling.

A typical efficiency of a binary power plant would be around 10% [21]. The reason for this low efficiency is mainly because this type of power plant is in most cases used with a geofluid at low temperature. But this can also be because of thermal loss in the heat exchanger.

There are some drawbacks for binary power plants to be used with a supercritical geofluid. The high pressures of the geofluid call for a very thick-walled heat exchanger. Since the minimum required temperature difference of geofluid and working fluid in a heat exchanger is proportional to the wall-thickness, this might call for an unattainable temperature difference, or inefficient heat transfer.

2.2 Corrosion and Erosion Problems in the Geothermal Industry

To fully discern the importance of the corrosion mitigation methods described later on, the reader must gain a good perspective on the actual problem, corrosion and erosion. In this section the chemistry behind the corrosion will be explained along with the way that erosion takes place.

Any acid is capable of inducing corrosion, but the following description shows how chloride can accelerates the process.

2.2.1 Chloride Induced Corrosion

Geothermal steam containing volatile chloride is found in steam fields throughout the world, such as Krafla in Iceland, Laraderello in Italy, Saint Lucia in Windward Islands, Tatun in Taiwan, and The Geysers in USA [18]. Most geothermal researchers agree that volatile chloride is transported as hydrogen chloride, HCl, although this has only been reported a few times [18].

When HCl comes in contact with water the compounds form chlorine and hydronium ions, as shown in the following reversible chemical reaction

$$HCl + H_2O \rightarrow H_3O^+ + Cl^- \tag{1}$$

HCl doesn't cause any considerable damage when the steam is above dew point, but when it goes below the acid dew point and the first droplets start to form in the gathering equipment, it dissolves the compound since it is so soluble. Hence, the droplets may contain thousands of ppm_w of HCl with pH levels below 2.0 units [17], causing a fast pitting corrosion. Stress corrosion cracking can also happen in the turbine, where cracks form at the bottom of a pit and propagate by corrosion fatigue leading to a final mechanical break [4]. HCl is usually only threatening when small amounts of liquid are present, since its concentration can be very high which accelerates the process of corrosion, but if large amounts of liquid are present then it will be diluted and not of any particular concern. It must also be taken into account that although the steam is highly superheated, there may be localized areas of heat loss where droplets can form, such as condensate pots and flanges.

It is the simultaneous attack of hydrogen and chloride ions that is especially damaging [10]. First, the chloride ion, with reference to equation 1, breaks the magnetite film on the metal surface inside the gathering equipment, Fe_3O_4, which protects the steel from damage of many other chemicals. This is shown in the following equation.

$$Fe_3O_4 + 8HCl \rightarrow FeCl_2 + 2FeCl_3 + 4H_2O \tag{2}$$

After the breaking of the film, the hydrogen ion has direct access to the metal and the actual

corrosion occurs by the following electrochemical reaction [17].

$$Fe + 2H^{+} \rightarrow Fe^{+2} + H_2 \tag{3}$$

The chloride ion does not participate directly in the corrosion, rather it accelerates the process. This happens both by electrically balancing the rapid build-up of positively charged metal ions as well as enhancement by migration of the ions beneath scale deposits, where the ions can hydrolyze, generating HCl [17]. This happens with the following chemical reaction, where the chlorine ions that initially parted from the hydrogen have reacted with iron(II), the product of the reaction shown in equation 3.

$$FeCl_2 + 2H_2O \rightarrow Fe(OH)_2 + 2HCl \tag{4}$$

The breaking of the magnetite film inside the gathering equipment, the neutralization of the buid-up of iron(II) (which, in other cases, hinders additional hydrogen ions to access the corrosion) and the production of more HCl (shown in equation 4) is what makes HCl especially problematic. It is therefore essential to both neutralize the acid and remove the chloride ions simultaneously [10].

It should be noted that these chemical reactions may vary, depending on other chemicals present in the steam, such as oxygen, ammonia, and boron for they may affect how the corrosion takes place.

An example of such a corrosion is in Krafla, Iceland. A well produced $20 - 100\text{ppm}_\text{w}$ chloride in superheated steam that resulted in corrosion rates of over 20mm/year. Excessive corrosion of 13% chromium steel turbine blade test coupons that were exposed to this steam was also observed [17]. While typical corrosion rates for carbon steel in gathering systems is around 0.1mm/year [13].

2.2.2 pH Buffers

The ideal pH level of water, that is being processed by traditional gathering equipment in the geothermal industry, has been determined to be around 8.0 units [17]. Adjusting the pH level of the acid droplets in the pipelines can be very difficult since there are many chemicals that work as pH buffers in the steam. Some common compounds affecting the pH level in geothermal steam are hydrogen chloride, hydrogen sulfide, boric acid, ammonia, and carbon dioxide [17].

2.2.3 Dew Point Corrosion

A dew point is the saturation temperature of a fluid in gas phase. Geothermal steam contains many different gases that each have a different dew point, some of which are higher than that of water vapor, such as H_2CO_4 [17]. That is, before water vapor, some other gases may codensate, that may be only a small fraction of the mass flow. This will produce a few droplets which may, as demonstrated above, dissolve chemicals such as HCl causing severe corrosion.

One way to prevent a dew point corrosion is to keep the steam above dew point temperature. This can often be very difficult for there are many factors that affect the dew point temperature.

2.2.4 Erosion in Gathering Equipment

In many cases, geothermal steam has entrapped small solid particles (dust), which may cause serious damage to gathering systems due to high velocities. Erosion, caused by these particles, may be detrimental to wellhead valves, fittings, and sharp bends in the pipelines [3]. These particles have more momentum than the steam, preventing them from taking sharp bends, in which they will slam into the pipeline wall and carve into the metal.

Cyclone separators are often used to remove particles from geothermal steam, preventing erosion. They make use of gravity and rotational effects in the way that the steam is forced to take sharp bends that the particles cannot reach because of their higher momentum. In the bends the particles are trapped and removed from the steam.

2.3 Corrosion Mitigation

It is important for the reader to know that there are many methods available in order to utilize a corrosive geofluid, each having its own advantages and drawbacks. The following is a short description of a few basic mitigation methods. These methods will be referred to later on in association with different power cycles described earlier.

2.3.1 Wet Scrubbing

Wet scrubbing is presently state of the art in heavy industry for cleaning flue gas [23]. It has been used for over 100 years with great success and undergone much development [2].

In the case of geothermal power plant working with steam containing volatile chloride, the basic technique is to inject liquid water with dissolved NaOH into the stream of superheated steam. The liquid cools the steam down to saturation, producing a liquid phase. After the HCl has dissolved in the liquid phase the following reactions take place.

$$NaOH + HCl \rightarrow NaCl + H_2O \tag{5}$$

The salt dissolves in the liquid phase and is removed from the system in the separator. The separators efficiency is very significant for the functionality of the scrubbing, for it has great effect on how much liquid carries over to the turbine. Small amounts of carryovers will evaporate in the downstream pipelines, while larger amounts can cause serious damage [2].

The water used for the scrubbing is often taken from the condenser where the steam is cooled down after expansion in the turbine. The injected water cools the steam down, resulting in loss of superheat. The mass of the injection liquid that enters the system makes for conservation of enthalpy, but the loss of the superheat leads to less recoverable energy.

It should be noted that other chemicals than NaOH can be dissolved in the injection liquid. NaOH will be used in this study for it has undergone the most development, is available in relatively high concentration, and is cheap.

2.3.2 Dry Steam Scrubbing

Dry steam scrubbing does not require any cooling of the superheated steam. Solid or liquid material is either injected to the stream in a length of a pipe along the pipeline or in a reactor vessel built into the pipeline [2]. When the chemicals are mixed with the flow, the fluid is driven through an electrostatic precipitator or a bag house filter where all the contaminants, along with the injected material, is filtered out [2]. The waste material can be recycled to lower operational costs and reduce waste.

There are two similar ways to implement this, absorption and adsorption. *Absorption* is a chemical reaction between the contaminants and the injected material(absorbent), while the surface of the *adsorbate* has fine pores that encloses the contaminants, not necessarily requiring direct chemical reaction. It is easier to recycle the adsorbent than the absorbent, which does not only lower operational costs but also cost of disposal [2].

Possible solid-phase absorbents to get rid of HCl are: Calcium carbonate ($CaCO_3$), calcium hydroxide ($Ca(OH)_2$), sodium carbonate (Na_2CO_3), zinc oxide (ZnO), sodium nitrate ($NaNO_3$), triazole ($C_2H_3N_3$), and amine. Possible solid-phase adsorbents to get rid of HCl are: Activated carbon, activated alumina, silica gel, and zeolites. [2]

A salt dissolved in water has strong electric fields that keeps the solution in liquid phase at conditions where water would normally evaporate. The solubility of a salt is proportional to the strength of the electric field, that is, as the solubility of a salt increases, it can coexist in liquid solution with a water vapor with a higher degree of superheat.

Potassium carbonate (K_2CO_3) is a salt with high solubility and can therefore coexist with superheated steam to some degree. Other compounds including potassium, e.g. KOH, could also be used, but K_2CO_3 is the safest to handle and is less bulky and cheaper. K_2CO_3 can coexist with steam to a degree of superheat much higher than NaOH, which is used in wet

scrubbing [15] [20].

K_2CO_3 can coexist with steam at much higher degree of superheat than $FeCl_2$ (see equation 4). That is, if K_2CO_3 is injected into superheated geothermal steam, it is certain that there will be a liquid phase of K_2CO_3 in the stream before H_2O, or other gases for that matter, would condense. The reaction between K_2CO_3 and HCl is the following.

$$K_2CO_3 + 2HCl \rightarrow 2KCl + CO_2 + H_2O \tag{6}$$

KCl cannot coexist with steam up to the same degree of superheat as K_2CO_3. This means that if the degree of superheat is high enough, KCl can dry out leaving solid particles in the stream. There are a few ways to prevent this; adding other salts and chemicals into the stream at the same time as K_2CO_3 will raise the temperature of precipitation of KCl, colder water can be injected into the steam to reduce the superheat to a degree that keeps KCl in liquid phase, or a crystal modifying agent or salt inhibitor can be applied to prohibit the precipitation [15].

Oil scrubbing is a special form of dry steam scrubbing. As the name implies, oil is injected into the superheated steam along a length of pipeline and either reacts with the unwanted chemicals or consumes them before entering the separator where it is parted from the steam.

Again the efficiency of the separator is very important. Oil that carries over to the turbine can cause very serious damage. It should be noted that the effect of the oil-carryover to the turbine and downstream processing equipment hasn't been properly studied [2].

Since oil boils at higher temperature than water, the injected oil has the potential of being much hotter than liquid water which results in less loss of superheat. If proper oil can be found, that reacts with the contaminants, this process has the potential to remove them while preserving up to 95% of the superheat [2]. Equipment to recycle the oil would both lower operational cost and prevent problems with disposal.

Since oil scrubbing has not been studied in details, it will not be a part of this study.

2.3.3 Binary Cycle

A heat exchanger that condenses a superheated geothermal steam containing HCl may suffer severe corrosion. The corrosion hasn't been eliminated, it may still take place inside the heat exchanger, depending on the material of construction.

The first droplets to form in the heat exchanger will have the effects described above. Although this might not actually be a corrosion mitigation, it is from the standpoint of the turbine and is worth looking into. The reason is that heat exchangers can tolerate the same rate of corrosion longer than turbines before breakdown, for they have no moving parts causing corrosion fatigue to accelerate the process. There is also more room for material selection when

constructing the instrument than in the case of turbines. Tests could be done to find the type of metal that can best withstand the corrosion.

It has to be noted that when handling the dry boreholes from the IDDP it is difficult, maybe even impossible, to keep the wellhead pressure of the geofluid such that it doesn't flash. The reason is that it seems that the steam in IDDP-1 is dry all out to the fractures in the rock outside the borehole. Which is why it is assumed that the heat exchanger will have superheated steam at the inlet and the corresponding condensate at the outlet.

2.4 Icelandic Deep Drilling Project

The IDDP is a consortium of three major energy companies in Iceland; Hitaveita Suðurnesja, Landsvirkjun, and Orkuveita Reykjavíkur along with the National Energy Authority of Iceland, Orkustofnun.

2.4.1 Goals

The goal is to access hydrothermal systems that are believed to exist under some of the high-temperature areas in Iceland. Reaching these systems will probably require boreholes that are 3-5km deep. The hope is to be able to extract superheated steam at subcritical pressure. It is expected that these systems will provide a steam with higher enthalpy and more mass flow rate than the high-temperature systems above them. Since power output is proportional to enthalpy and mass flow rate, the result would be more powerful boreholes.

This will not only increase expectation on the development of geothermal energy in Iceland, but also globally. This will increase the output potential of high temperature geothermal reservoirs. Consequently, geothermal power would increase its share in the global electricity production and meet demand that might otherwise be met with other more polluting energy sources. If the IDDP is successful it will have both positive effects on the environment as well as yielding scientific benefits.

The International Scientific Continental Drilling Program (ICDP) consists of Icelandic and foreign parties that take part in the planning of the IDDP and has granted the IDDP a financial support and has held a few workshops around the program.

2.4.2 IDDP-1

After a lot of preparation, the first borehole, IDDP-1, was constructed at Krafla Power Station in the north of Iceland. It was originally meant to be 4.5km deep, but the drilling operation ended in a magma intrusion at a depth of 2.104km. After two failed attempts to sidetrack the bore to get past the intrusion, the drilling was stopped. [22]

In july, the following year, a flow test was executed giving surprising results. It turned out that the borehole provided dry steam with much higher enthalpy than expected, close to $3100\text{kJ}/\text{kg}$. There have been a lot of difficulties with the borehole and operators have never been able to keep it open in order to get a stable flow; it is constantly changing its behavior. [7]

Results from a chemical analysis of the steam from IDDP-1 show that after the fluid became dry, the chloride concentration seemed stabilized at $50 - 65\text{ppm}_\text{w}$ [12]. During flow tests, the wellhead suffered severe corrosion and erosion, especially in bends. This caused many problems that have, in all cases, led to termination of the tests. This is the reason for why the borehole has never reached equilibrium.

While the borehole is kept closed, the borehole casing seems to be undergoing corrosion. This was inferred from the fact that chunks of steel had been coming to surface shortly after the hole was opened, also the steam stroke was black because due to FeOS particles, entrapped in the steam. To prevent corrosion in the surface casing, the borehole has to be able to bleed at all times. Bleeding is when the mass flow rate is kept at the minimum required to keep the steam dry, keeping the casing from experiencing more damage.

2.4.3 Future

The program participants intend to drill two boreholes, IDDP-2 and IDDP-3, in 2011-2015. IDDP-1 is situated at Krafla power station which is a property of Landsvirkjun, so IDDP-2 and IDDP-3 will be at the Hengill and Reykjanes area, which Orkuveita Reykjavíkur and Hitaveita Suðurnesja have the right to utilize.

3 Method

This analysis is twofold. One part examines what corrosion mitigation method is best to exploit IDDP-1, whilst the other analyzes the methods in general, with respect to enthalpy and power output. The goal of the latter part is to map the applicability of each method to help future decision makers determine which method is best suited for their circumstances. In this study six software models are constructed and compared.

One model is of a dry steam power cycle with no corrosion mitigation. In reality, this power cycle would suffer excessive corrosion but is interesting for comparison with the alternatives. Three different implementations of a single flash cycle with wet scrubbing are modeled. Each having different components in the power cycle that affect the power output. One implementation of a dry steam cycle with dry scrubbing is modeled. And finally, a binary power cycle is modeled with water as a working fluid.

Three additional models of a binary cycle were constructed, using isopentane, isobutane, and ammonia as working fluids. These models will not be a part of this study for they had much lower utilization efficiency and power output than the one with water as working fluid, as expected. Working fluid selection depends largely on finding the fluid with critical temperature closest to the temperature of the geofluid at the wellhead; these three fluids do not fulfill this criterion. They are not believed to contribute to the study.

This chapter will first show how important processes in the methods are modeled, and then describe each method in more detail.

3.1 Energy Conversion Processes

This section describes how individual thermodynamic processes that are important for each power cycle are implemented in the corresponding model, and elaborates on which assumptions and approximations are made.

3.1.1 Separation

The separation process is modeled as an isobaric process. The quality of the stream at state 1, referring to Figure 4, is used to find what fraction of the stream, $\dot{m}_2$, goes towards the turbine, as shown in the following expression.

$$\dot{m}_2 = x_1 \dot{m}_1 \tag{7}$$

3.1.2 Turbine Expansion

Wet Expansion The conversion of thermal energy to mechanical energy takes place when the fluid expands through a turbine. Heat transfer between the turbine and its surroundings is ignored, as are kinetic and potential energy effects. The work produced, with reference to Figure 4, is given by

$$\frac{W_t}{\dot{m}} = (h_2 - h_3) \tag{8}$$

Since state 2 and $\dot{m}_2$ are fixed, the work depends on the value of h_3, and increases as h_3 is reduced. The maximum allowed turbine work can be determined using the second law of thermodynamics.

Because the entropy production cannot be negative, the only states that can actually be attained adiabatically are those with $s_3 > s_2$. The state labeled as 3_s could be attained only in the limit of no internal irreversibilities, that is, with an isentropic expansion through the turbine. With a fixed pressure at the turbine outlet, h_3 decreases with the specific entropy s_3. In other words, the smallest allowed value for h_3 corresponds to s_{3s}.

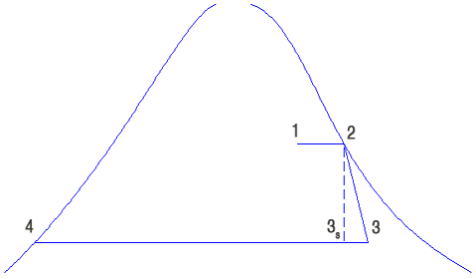

Figure 4: Temperature-entropy diagram showing the process that a stream undergoes during separation, wet turbine expansion, and condensation.

In an actual turbine expansion less work than the maximum is attained for $s_3 > s_{3s}$. This difference is measured by the isentropic turbine efficiency defined by the following equation [14].

$$\eta_t = \frac{h_2 - h_3}{h_2 - h_{3s}} \tag{9}$$

When the fluid entering the turbine is saturated vapor, the Baumann rule is used in order to account for degradation in performance of the turbine due to moisture which is present during the expansion; the higher the moisture, the lower the efficiency [21]. Involving the Baumann rule, the isentropic efficiency for a turbine operating with wet steam is

$$\eta_{tw} = \eta_{td} \frac{1 + x_3}{2} \tag{10}$$

where the isentropic efficiency for a turbine operating with dry steam, η_{td}, is assumed to be constant at 85%, throughout this study.

The turbine outlet pressure, p_3, is determined by the condenser temperature. The corresponding specific enthalpy of saturated vapor and liquid, h_{3g} and h_{3f} respectively, are found

from steam tables, and h_{3s} is calculated by

$$h_{3s} = h_{3f} + x_{3s} h_{3fg} \tag{11}$$

where x_{3s} is

$$x_{3s} = \frac{s_2 - s_{3f}}{s_{3fg}} \tag{12}$$

and h_{3fg} is

$$h_{3fg} = h_{3g} - h_{3f} \tag{13}$$

The following equation is used to determine the enthalpy of the stream at the turbine outlet [21].

$$h_3 = \frac{h_2 - 0.425(h_2 - h_{3s})(1 - \frac{h_{3f}}{h_{3g} - h_{3f}})}{1 + \frac{0.425(h_2 - h_{3s})}{h_{3g} - h_{3f}}} \tag{14}$$

Now, the work produced by the turbine can be computed with equation 8.

Dry Turbine Expansion When the fluid entering the turbine is superheated steam, the modeling is carried out in a different way, for at some point in the turbine expansion, the vapor will cross the saturation curve, changing the properties of the expansion. In the modeling, the expansion is split in two parts and is referred to as dry expansion and wet expansion. Where the latter is the part after the properties have crossed the saturation curve.

The pressure at state 2, referring to Figure 5, where the properties of the fluid cross the saturation curve is found by trial-and-error. A reasonable pressure level is guessed and the corresponding specific enthalpy of saturated vapor and liquid, h_{2g} and h_{2f} respectively, are found from steam tables, and h_{2s} is calculated as shown above.

The efficiency of the expansion is then calculated with the following equation.

$$\eta_{td} = \frac{h_1 - h_{2g}}{h_1 - h_{2s}} \tag{15}$$

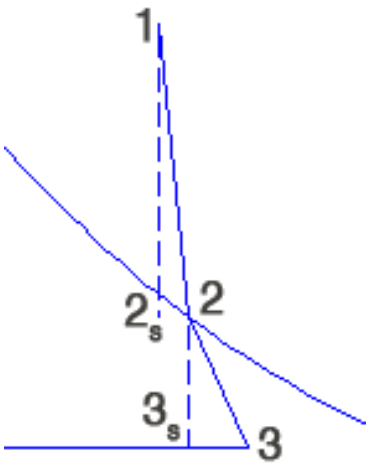

Figure 5: Temperature-entropy diagram showing the how the steam crosses the saturation curve between dry and wet turbine expansion.

If η_{td} is not 85%, another pressure is guessed and the calculation repeated. When the pursued pressure has been found, the power output from the wet expansion is found as described above. The total specific power output from the expansion is

$$\frac{W_t}{\dot{m}_{gf}} = (h_1 - h_2) + (h_2 - h_3) \tag{16}$$

where $\dot{m}_{gf}$ is the mass flow rate of the geofluid.

For both wet and dry turbine expansion, the back pressure of the turbine is 0.1bar. This gives a steam quality between 74 to 87%.

3.1.3 Condensation

After both temperature and pressure of the stream have dropped during the turbine expansion, the fluid enters the condenser. At this stage the fluid is a mixture of saturated vapor and saturated liquid. The steam is cooled down in the condenser by rejecting heat to a cooler medium whose temperature increases. The fluid leaves the condenser at state 4 as saturated liquid, see Figure 6 and 4. At steady state, mass and energy balances for a control volume enclosing the condensing side of the heat exchanger give

$$\frac{Q_{out}}{\dot{m}_{gf}} = h_3 - h_4 \tag{17}$$

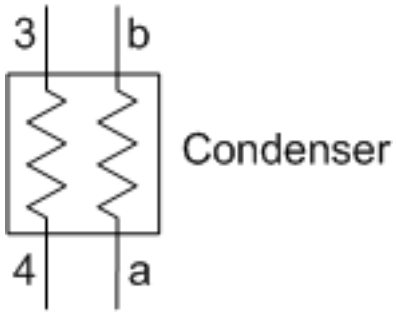

Figure 6: Process diagram for the condenser.

where $Q_{out}/\dot{m}_{gf}$ is the rate of heat transfer from the geofluid to the cooling medium. [14]

At steady state, mass and energy rate balance for the control volume enclosing the cooling medium side of the condenser gives

$$\frac{Q_{in}}{\dot{m}_{cm}} = h_b - h_a \tag{18}$$

Energy balance across the condenser gives that $Q_{out} = Q_{in}$, which again gives

$$\dot{m}_{gf}(h_3 - h_4) = \dot{m}_{cm}(h_b - h_a) \tag{19}$$

3.1.4 Cooling Tower

A wet cooling tower is used to cool the medium in the condenser. The waste heat is rejected to the atmosphere with cooling medium (in this case; water) recirculating and serving as a transport medium for the heat transfer between the source (geofluid) and the sink (atmosphere) [26].

A wet cooling tower is an evaporative cooler with an induced-draft counterflow. A fan at the top of the tower draws air in from the bottom. The recirculating cooling water is sprayed down the cooling tower from the top. During this process, a part of the cooling water evaporates, which cools the remaining water while the temperature and moisture content of the atmosphere increases. The cooling water is collected at the bottom of the tower and then pumped back into the condenser. Since part of the cooling water evaporates, makeup water is added to the cycle to keep the process going.

Energy and mass balance have to be evaluated in order to determine the mass flow of air required to cool the cooling water.

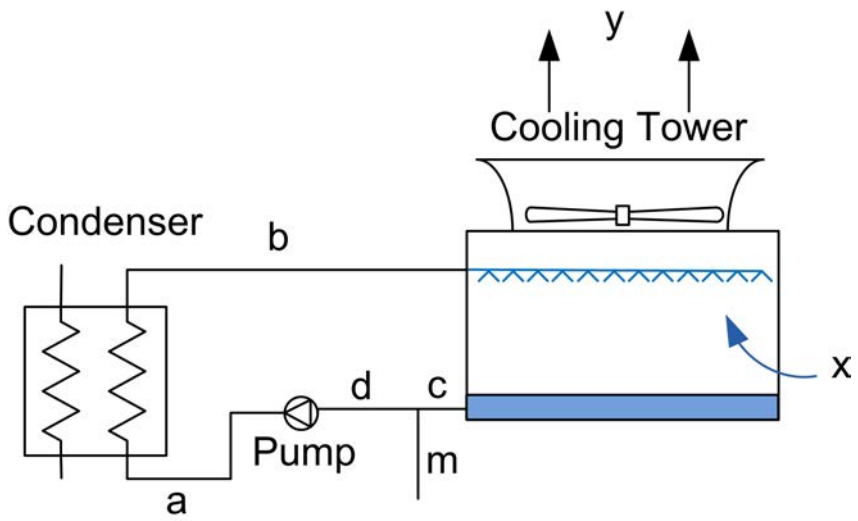

Figure 7: Process diagram for a cooling tower.

Applying the fist law of thermodynamics to the cooling tower gives the following relation, assuming steady flow and overall adiabatic condition, with reference to Figure 7.

$$\dot{m}_b h_b + \dot{m}_x h_x = \dot{m}_c h_c + \dot{m}_y h_y \tag{20}$$

In order to account for the evaporation of the cooling water and the corresponding water uptake of the air, the mass conservation of water and air is evaluated, and is given by

$$\dot{m}_b + \dot{m}_{wx} = \dot{m}_c + \dot{m}_{wy} \tag{21}$$

and

$$\dot{m}_{ax} = \dot{m}_{ay} \tag{22}$$

Where the former equation shows mass conservation of water, and the latter mass conservation of day air. $\dot{m}_{w-}$ represents the water content of the corresponding stream and $\dot{m}_{a-}$ represents the dry air content of the corresponding steam. The water content of the atmospheric streams are found with the specific humidity, ω.

$$\dot{m}_{wx} = \omega_x \dot{m}_x \tag{23}$$

and

$$\dot{m}_{wy} = \omega_y \dot{m}_y \tag{24}$$

Cooling towers are characterized by many parameters where range and approach are important and are often used to determine the cooling towers performance. Range is the temperature difference between the cooling water entering and leaving the cooling tower. Approach is the temperature difference between the cooling water leaving the tower and the ambient wet bulb temperature. As a general rule, the cooling tower becomes more expensive as the approach gets smaller, due to necessary increase in its size.

A cooling tower is designed to cool a certain amount of cooling water to a certain temperature. Since the wet bulb temperature is the theoretically lowest temperature that the cooling tower can cool the cooling water down to, that is one of the most important factors to consider, for it is determined by the environment, not the designer. As a general rule, the design wet bulb temperature should not be exceeded for more than five percent of the time. [24]

Using data from the Icelandic Met Office for a weather station situated at Bjarnarflag, around 8km south of IDDP-1, it was calculated that the temperature exceeded $14.5°C$ only five percent of the time. On these days the average relative humidity was 60.7%, giving a corresponding wet bulb temperature of $10.5°C$. Based on this, it is determined that the cooling tower is to get the temperature of the cooling water down to $20°C$; giving an approach of $9.5°C$ on the hottest days.

With regard to the geofluid temperature of $48°C$ at the condenser inlet, the hotter tem-

perature of the cooling water is determined to be $40°C$. The range of the cooling tower is consequently $20°C$.

When calculating the required mass flow rate of air through the cooling tower in order to determine its use of electricity, the average temperature over the last four years and the corresponding relative humidity are used. Those are calculated to be $2.5°C$ and 76%, respectively.

Electricity consumption of the fan in the cooling tower is evaluated by finding the energy required to raise the calculated mass flow rate of air through the cooling tower. The following equation is used as an approximation; it neglects all resistance due to turbulence and fill inside the cooling tower.

$$W_{CT} = H * \dot{m}_{air} * g * \eta_{fan} \tag{25}$$

Where the fan efficiency, η_{fan}, is assumed to be 70% [25], and H is the height of the cooling tower.

3.1.5 Heat Exchanger in a Binary Cycle

The analysis of the heat exchanger in a binary cycle is a straightforward application of the principles of thermodynamics and mass conservation. Changes in kinetic and potential energies are neglected, as well as heat transfer to the surroundings. Also, the heating/cooling process that the fluids at either side of the heat exchanger are undergoing will be assumed to be isobaric.

The governing energy balance for the heat exchanger, with reference to Figure 18, is

$$\dot{m}_{gf}(h_1 - h_4) = \dot{m}_{wf}(h_b - h_e) \tag{26}$$

Where $\dot{m}_{gf}$ is the mass flow rate of the geofluid and $\dot{m}_{wf}$ is the mass flow rate of the working fluid.

When modeling a heat exchanger for a binary cycle that allows the working fluid to superheat, the instrument is divided into three parts; preheater, evaporator, and superheater. These names are given in terms of what thermodynamic process the working fluid is undergoing at each time.

The working fluid enters the preheater at state b, in liquid form, and heats up to the saturated liquid curve, state c. As the name implies, the working fluid evaporates in the evaporator up to the saturated vapor curve, state d. Since the geofluid has a considerate degree of superheat, the superheater is used to heat the steam even more, to state e. The reason for this division of the heat exchanger up to three parts during modeling is to ensure that the temperatures of the geofluid are greater than of the working fluid at all stages.

Knowing the properties of the fluids at states 4, b and c, the properties of the geofluid at state 3 are found with the following energy balance across the preheater.

$$\dot{m}_{gf}(h_3 - h_4) = \dot{m}_{wf}(h_c - h_b) \tag{27}$$

Using the known properties at states 3, c and d, the properties of the geofluid at state 2 are found with the following energy balance across the evaporator.

$$\dot{m}_{gf}(h_2 - h_3) = \dot{m}_{wf}(h_d - h_c) \tag{28}$$

After finding the properties of the fluids at these states, it can be verified that the geofluid is at higher temperatures than the working fluid at all times. The pinch point of the heat exchanger never goes below $5°C$. A pinch point is the smallest temperature difference between the two fluids in the heat exchanger.

Evaluation of the area of the heat exchanger includes two different overall heat transfer coefficients. For the PH and EV the coefficient is taken as $1200\mathrm{W/m^{2\circ}C}$ [8]. In the superheater, where both sides of the heat exchanger have superheated steam, the coefficient had to be calculated from scratch, for it wasn't found elsewhere. Neglecting conduction resistance in the steel pipe and area difference between the two sides of the heat exchanger and assuming that the heat transfer coefficient is the same on both sides, the equation for calculating overall heat transfer coefficient can be simplified as following [8].

$$U = \frac{1}{1/h_i + (A_i ln(r_o/r_i))/(2\pi kL) + (A_i/A_o)(1/h_o)} = \frac{h}{2} \tag{29}$$

Using steam at temperature and pressure of $300°C$ and 50bar, respectively, flowing at $30m/s$ and a pipe diameter of 25mm, the heat transfer coefficient is found to be $\mathrm{h} = 170\mathrm{W/m^{2\circ}C}$ giving an overall heat transfer coefficient of $\mathrm{U} = 85\mathrm{W/m^{2\circ}C}$. This overall heat transfer coefficient is used to evaluate the area of the SH.

3.1.6 Feed Pump in a Binary Cycle

In order for the working fluid to be able to expand in a turbine repeatedly, its pressure has to be raised with a pump after each expansion. Heat transfer between the pump and its surroundings are ignored, as are kinetic and potential energy effects. The work, W_p required to raise the pressure of the working fluid between points a and b, with reference to Figure 18, is given by

$$\frac{W_p}{\dot{m}} = h_b - h_a \tag{30}$$

Since state a and $\dot{m}$ are fixed, the work depends on the value of h_b, and decreases as h_b

is reduced. The minimum allowed work required can be determined by the second law of thermodynamics.

Since entropy production cannot be negative, the only states actually attainable are those where $s_b > s_a$. The state where $s_b = s_a$, referred to as s_{b_s} could be attainted only in the limit of no internal irreversibilities, that is, with an isentropic compression in the pump. With a fixed pressure at the pump outlet, h_b decreases as the specific entropy s_b decreases. In other words, the smallest allowed value for h_b corresponds to the state where $s_b = s_a$.

In an actual pump compression, more work is required since the process is not isentropic. The isentropic efficiency of the pump, 80%, is used to calculate h_b with the following expression.

$$\eta_p = \frac{h_b - h_a}{h_{b_s} - h_a} \tag{31}$$

3.1.7 Injection of Alkali Liquid in Wet Scrubbing

In order to apply wet scrubbing on superheated steam, it has to be cooled down to a state where its quality is approximately 98% [18]. This produces a liquid flow, equal to 2% of the steam flow, out of the separator.

The following energy balance for the node 1-2-7, with reference to Figure 11, is used to determine how much water at T_7 is required in order to get the desired quality at state 2. The cooling is assumed to be isobaric and adiabatic.

$$\dot{m}_1 h_1 = \dot{m}_2 h_2 + \dot{m}_7 h_7 \tag{32}$$

This energy balance shows that although the steam is colder at state 2 than state 1, the increase in mass flow rate makes for conservation of enthalpy. The following expression gives the exergy of a system at a given state, neglecting kinetic, potential, and chemical exergy [14]. It shows that although the enthalpy is conserved, the cooling of the steam causes exergy destruction due to change in entropy, but is partly compensated by the increase in mass flow rate.

3.1.8 Exergy Analysis

Exergy analysis is one way to discern losses in a power cycle. The exergy of the geofluid at the each state in the power cycle is found using equation 33, where the *dead state* is liquid water at atmospheric pressure and $2.5°C$. Knowing these values, the calculations are a straightforward application of addition and subtraction to determine the losses between each state.

$$E = \dot{m}(h - h_0 - T_0(s - s_0)) \tag{33}$$

Both the geofluid and injection fluid, where appropriate, are taken as inputs to the system, while electricity consumption of pumps and cooling tower fan are taken as outputs.

The exergy analysis is applied on the case of IDDP-1, with a wellhead pressure of 50bar.

3.2 Description of Individual Models

This section describes, step by step, how each method is modeled. It lists the processes that each method consists of, and shows the combination of power cycles and corrosion mitigation methods.

3.2.1 Dry Steam Cycle without Corrosion Mitigation

A process diagram and the corresponding T-s diagram of the power cycle are shown in Figures 9 and 8, respectively.

The superheated steam is led into a steam turbine where the expansion begins dry but crosses the saturation curve and becomes wet, and takes place as described in section 3.1.2

After that the fluid enters the condenser and undergoes a process as described in section 3.1.3. A description of the cooling tower can be found in section 3.1.4.

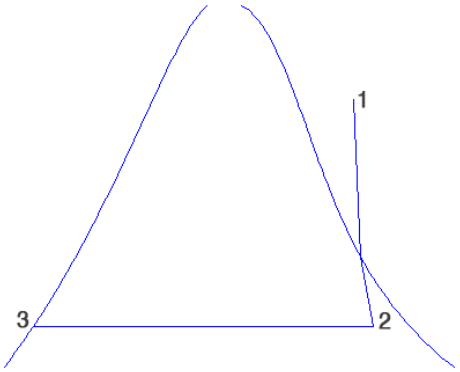

Figure 8: Temperature-entropy diagram of a dry steam power cycle.

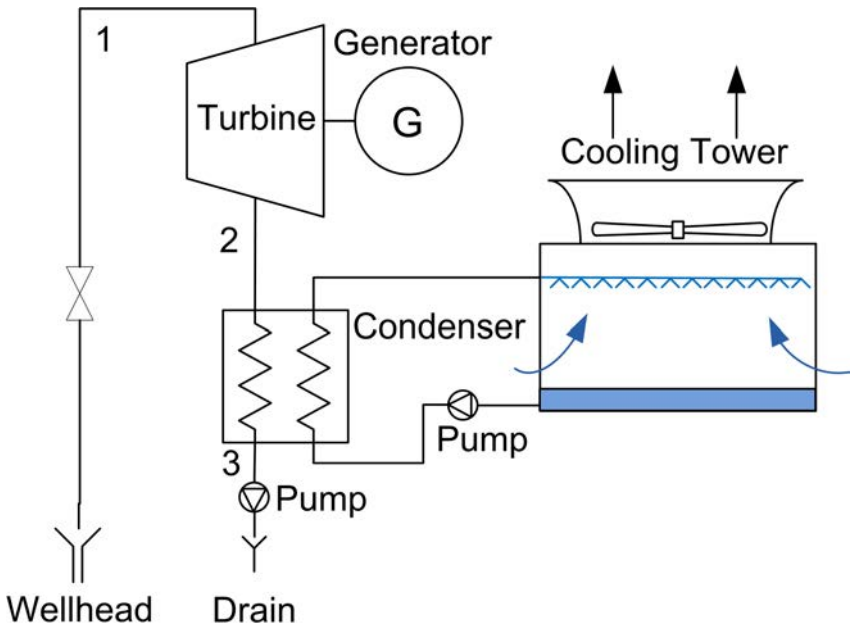

Figure 9: Process diagram of a dry steam power cycle.

3.2.2 *Single-Flash Cycle with Wet Scrubbing*

A process diagram and the corresponding T-s diagram of the power cycle are shown in Figures 11 and 10, respectively.

Before the superheated steam enters the separator in the power cycle, enough liquid water is injected into the steam to cool it down, isobarically, to a point where its quality is 98%. This is process is described in section 3.1.7. As described in section 2.3.1, the injected water contains dissolved NaOH in order to fight corrosion.

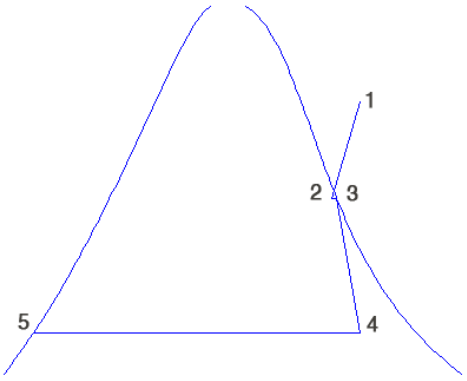

Figure 10: Temperature-entropy diagram of a single flash power cycle with wet scrubbing.

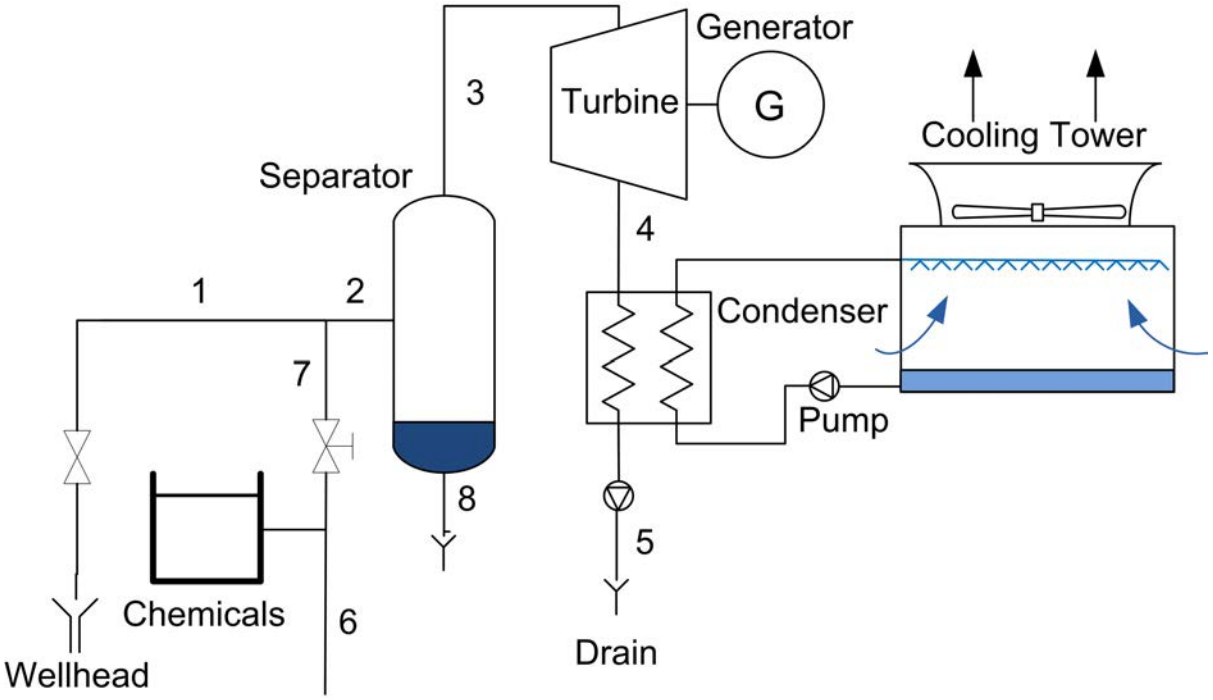

Figure 11: Process diagram of a single flash power cycle with wet scrubbing.

After that the fluid undergoes separation as described in section 3.1.1. Since the liquid at state 3 contains no significant superheat, the turbine expansion is assumed to be solely wet. Such an expansion is described in section 3.1.2

Next, the fluid enters the condenser and undergoes a process as described in section 3.1.3. A description of the cooling tower can be found in section 3.1.4.

Figure 10 shows the entropy destruction that takes place during wet scrubbing which affects the exergy of the geofluid. This applies to all implementations of wet scrubbing.

3.2.3 Single-Flash Cycle with Wet Scrubbing and Heat Recovery

Before the superheated steam undergoes traditional wet scrubbing, it enters a heat exchanger where it cools down isobarically. This is a steam-only heat exchanger which might require a very large surface area and could be hard to construct due to thick walled piping required to withstand the high pressures, and also provide a suitable corrosion allowance. This study will not cover that in more detail, and from this point on it is assumed that the equipment is available.

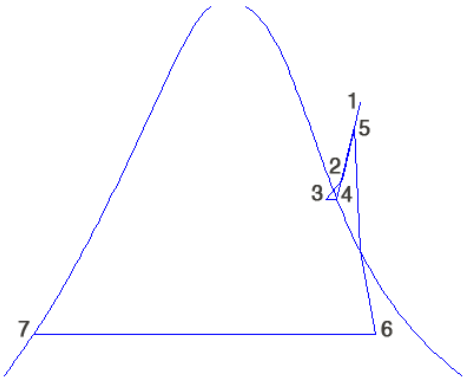

Figure 12: Temperature-entropy of a single flash power cycle with wet scrubbing and heat recovery.

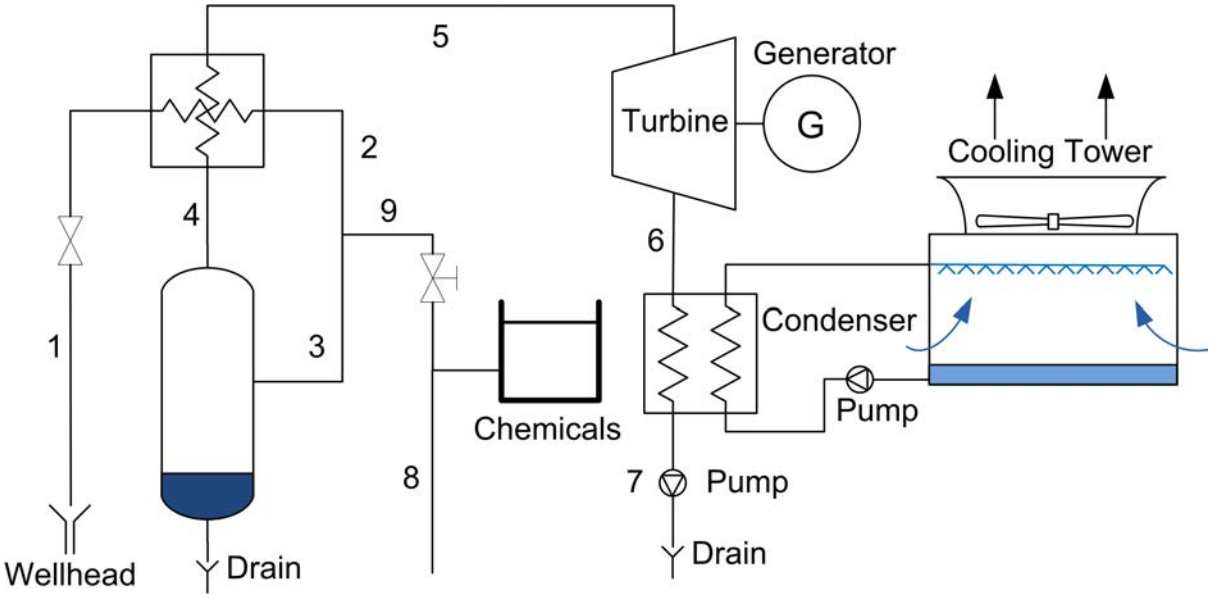

Figure 13: Process diagram of a single flash power cycle with wet scrubbing and heat recovery.

At the outlet of the heat exchanger, the fluid has $20°C$ of superheat, which is enough to ensure that no condensation takes place. Figure 13 and 12 show a schematic diagram and the corresponding T-s diagram of the power cycle. Knowing the pressure and temperature at point 2, the corresponding enthalpy is found from steam tables.

Next, enough liquid water is injected into the steam to cool it down, as demonstrated in section 3.1.7.

The pressure and quality at state 4 are used to find the temperature and enthalpy of the steam from steam tables, and $\dot{m}_4$ is found by

$$\dot{m}_4 = x_3 \dot{m}_3 \tag{34}$$

When the stream has undergone separation, as described in section 3.1.1, the steam enters the heat exchanger and gains superheat again. The following energy balance is used to calculate the enthalpy of the stream at state 5.

$$\dot{m}_1(h_1 - h_2) = \dot{m}_4(h_5 - h_4) \tag{35}$$

Expansion of superheated steam in the turbine is described in section 3.1.2.

After that the fluid enters the condenser and undergoes a process as described in section 3.1.3. A description of the cooling tower can be found in section 3.1.4.

In the evaluation of the heat exchangers area, an overall heat transfer coefficient of $85\mathrm{W/m^2{}^\circ C}$ is used. Derivation of the coefficient was shown in section 3.1.5.

Since the steam does not condense in the heat exchanger, it is assumed that it is made of stainless steel.

3.2.4 Single-Flash Cycle with Wet Scrubbing and an Additional Turbine

Before the superheated steam enters the traditional setup of wet scrubbing, it expands through a turbine without condensing. A process diagram and the corresponding T-s diagram are shown in Figures 15 and 14, respectively. At the turbine outlet, the fluid has $20^\circ C$ of superheat, which is enough to ensure that no condensation takes place. The turbine expansion is similar to the one described in section 3.1.2. The difference is that this is solely a dry expansion, and in order to keep a $20^\circ C$ superheat at the turbine outlet, the pressure at which the fluids properties would have crossed the saturated vapor curve is raised so that the temperature is $20^\circ C$ higher.

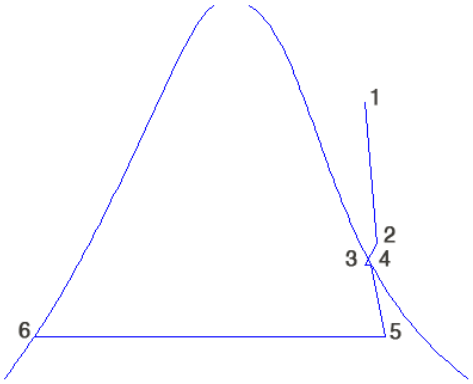

Figure 14: Temperature-entropy diagram of a single flash power cycle with wet scrubbing and an additional turbine.

After the steam has expanded through the turbine it undergoes wet scrubbing as described in section 3.1.7. It then enters the separator and expands through a turbine as described in

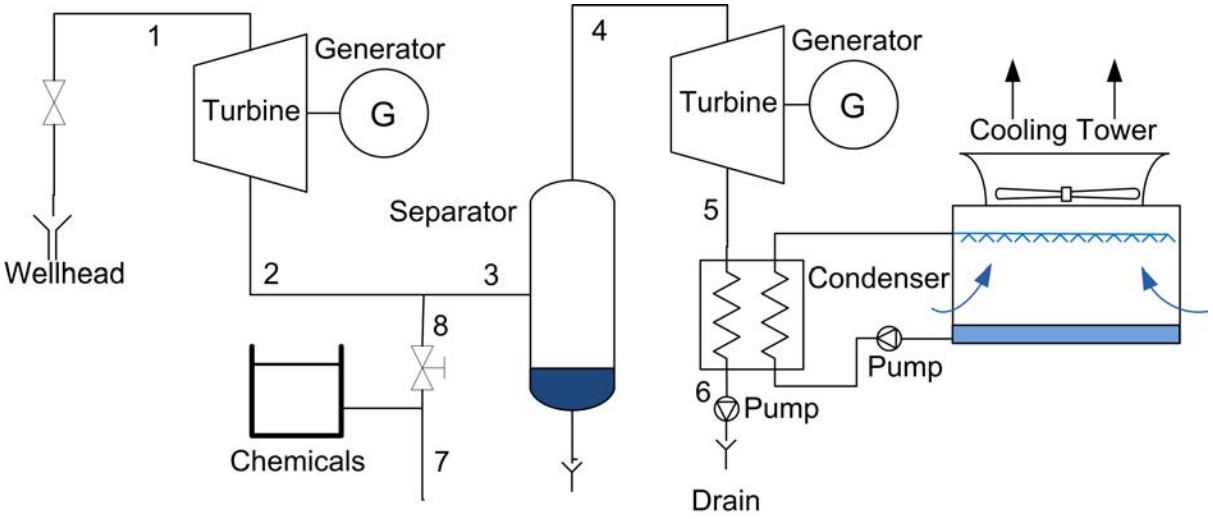

Figure 15: Process diagram of a single flash power cycle with wet scrubbing and an additional turbine.

sections 3.1.1 and 3.1.2, respectively. At last the fluid condenses, as described in section 3.1.3. A description of the cooling tower can be found in section 3.1.4.

3.2.5 Dry Steam Cycle with Dry Steam Scrubbing

A process diagram and the corresponding T-s diagram of the power cycle are shown in Figures 17 and 16, respectively.

The superheated steam at state 1, enters a reaction vessel. The reaction vessel is a reference to any sort of equipment where chemicals are injected into the stream and react with or consume (absorption or adsorption) the HCl, where the injected material is in solid or liquid form. The mixed flow is then passed through some sort of separator, such as a bag house filter or electrostatic precipitator. The spent reactant may then be recycled after being separated from the steam [2].

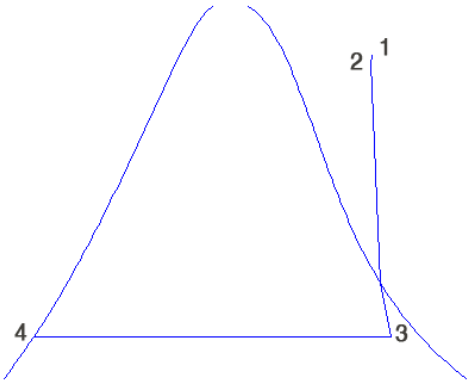

Figure 16: Temperature-entropy diagram of a dry steam cycle with dry steam scrubbing.

It is hard to estimate the losses in this setup, since it has not been applied often, therefore it is assumed that they are similar to the ones in the laboratory bench tests that were conducted at Thermochem Laboratories in California, USA. The total heat loss for the processes ranged from $0-0.5\%$, in this case they are assumed constant at 0.5%. Also, the total pressure drop was 0.14bar and that is also assumed constant. There was no measurable reduction in mass

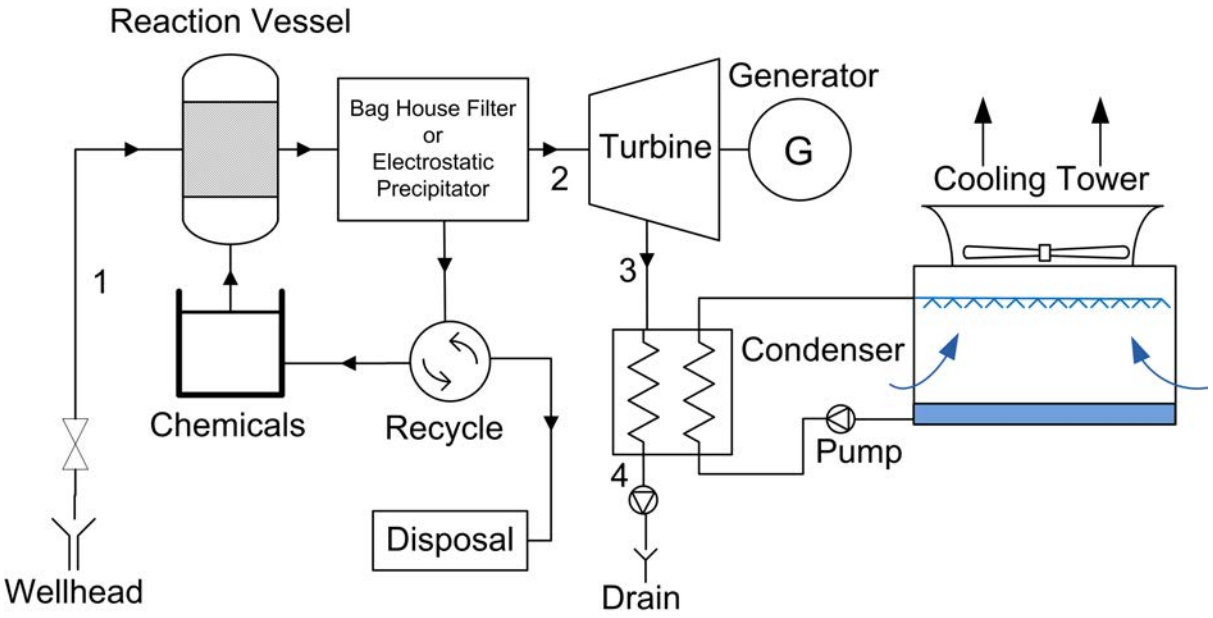

Figure 17: Process diagram of a dry steam cycle with dry scrubbing.

flow. [19]

After this, the geofluid expands through the turbine as described in section 3.1.2. After that it is cooled down as shown in section 3.1.3. The cooling tower process is described in section 3.1.4.

The author did not find enough articles that commented on the recycling of the used reactant in order to give a fully supported description. It will have to suffice to say that it is possible to recycle the reactant, and some reactant materials are better suited for recycling than others [2]

3.2.6 Binary Cycle with Condensation of Geofluid in Heat Exchanger

A process diagram and the corresponding T-s diagram of the power cycle are shown in Figures 19 and 18, respectively.

The process that takes place in the heat exchanger in the binary cycles is described in detail in section 3.1.5. After the working fluid has received heat from the geofluid, it expands through a turbine as demonstrated in section 3.1.2. After that it is cooled down and pumped up to a higher pressure, as shown in sections 3.1.3 and 3.1.6, respectively. The cooling tower process is described in section 3.1.4.

In order for the heat exchanger in the binary cycle

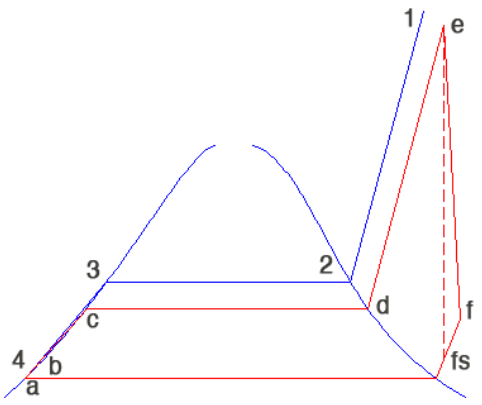

Figure 18: Temperature-entropy diagram of a binary cycle.

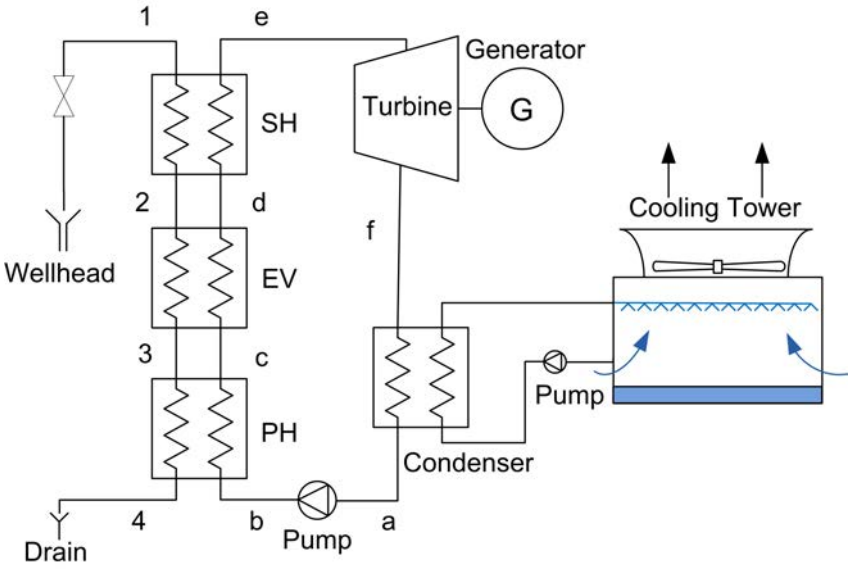

Figure 19: Process diagram of a binary cycle.

to withstand corrosion it has to be constructed from certain alloys. Determination of what alloy does best withstand the attack of HCl is not part of this study. But for the sake of performing economic analysis, a heat exchanger made of titanium is assumed to be the best choice.

3.3 Economic Analysis

In order for the reader to get a feeling for the economical feasibility of each corrosion mitigation, a simple economic analysis is carried out.

For IDDP-1, the overnight capital cost of a power plant using a dry steam cycle without any corrosion mitigation system is used as a reference point, and is considered to be $\$2500/\text{kW}$. Overnight capital cost is the total capital cost assuming that the power plant would be built overnight. Other power cycles on the same geothermal field that produce less power cannot use the same value for capital cost, since the well field costs would be the same regardless of the power output. Therefore a 0.6 exponent is introduced.

As an example, a dry steam cycle with a turbine of A kW would cost $\$2500 * \text{A}$. Another power cycle, working on the same well field, with a turbine of B kW and a corrosion mitigation system that costs \$X would have a total capital cost of $\$2500(\text{A}/\text{B})^{0.6}\text{B} + \text{X}$.

Economic analysis for hypothetical geothermal wells, producing steam that carries the same amount of HCl as IDDP-1, is carried out slightly differently. It is assumed that two wells, both producing steam at $50bar$ but one with steam at enthalpies of $2900\text{kJ}/\text{kg}$ and the other of $3600\text{kJ}/\text{kg}$, have the exact mass flow rate to produce 50MW of electricity with a dry steam power cycle without corrosion mitigation. The mass flow rate, along with the specific power for each corrosion mitigation method shown below, is used to calculate the power output of each method. The costs are calculated in the same way as for the case of IDDP-1.

Monthly operational and maintenance costs are assumed to be $0.45/\text{kW}$ for both cases. For a power cycle using wet scrubbing, the operational cost is slightly higher. At the Aidlin power plant in the Geysers, USA, the monthly operational cost for cleaning 30ppm of HCl from a steam flow of $50\text{kg}/\text{s}$ using NaOH was $\$5,800$ [19].Taking into account the fact that IDDP-1 contains twice the amount of HCl, the additional operational cost of wet scrubbing is considered to be \$11,600

Switching from wet scrubbing to dry scrubbing using $CaCO_3$ at the Aidlin power plant was estimated to lower operational costs to \$2500 [19]. Again, taking into account the difference in amount of HCl, this is considered to be \$5,000.

The following equations are used as an approximation to calculate the cost of a heat exchanger made of stainless steel and titanium, respectively, where A is the area of the equipment in m^2 [11].

$$cost[\$] = 3.5 * A^{0.8} * 1,300 \tag{36}$$

$$cost[\$] = 5,0 * A^{0,8} * 1,300 \tag{37}$$

In order to estimate the cost of the additional turbine in one implementation of wet scrubbing, a 45MW turbine (including generator and controls) is considered to cost $\$18 * 10^6$. The following equation is used to scale the cost for other MW ratings [1].

$$Scaled\ \ cost = \$18 * 10^6 (\frac{new\ \ MW\ \ rating}{45MW})^{0.9} \tag{38}$$

The cost of installing wet scrubbing and dry steam scrubbing is estimated to be \$200.000 and \$1.000.000, respectively, regardless of enthalpy and pressure. There is not much data available to perform a good cost estimation of the installing cost of the scrubbing technologies, this is considered acceptable for this study.

3.4 Design Criteria for Modeling of IDDP-1

In order to analyze which corrosion mitigation method is best for IDDP-1 the input parameters in the models mimic the ones of the borehole.

The enthalpy at the wellhead has been measured to be around $h_{wellhead} = 3100kJ/kg$ for different pressures, which will be taken as a constant for the IDDP-1 case.

To realize the order of magnitude of extractable power output from IDDP-1, the mass flow rate profile of the borehole is needed. The mass flow rate profile shows the relation between mass flow rate of the geofluid with respect to wellhead pressure. Because of all the troubles that where described in section 2.4.2, the borehole has never been at complete steady state. This entails that there is no good mass flow rate profile available for the borehole.

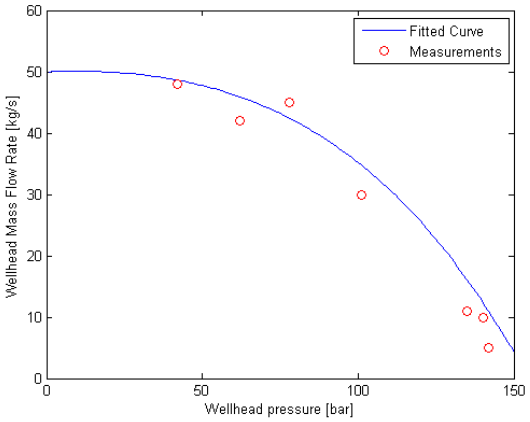

Figure 20: Measured mass flow rate at IDDP-1 in August 2011. The figure also shows a curve that has been fitted to the data.

The best data available for the mass flow rate profile of the borehole where collected in August, 2011. These measurements are shown in Figure 20. The figure also shows a curve that has been fitted to the date in order to get a better spectrum of the flow rate profile. The MATLAB *Basic Fitting Tool* was used to fit the measured data with an exponential function.

3.5 Examination of the Methods Applicability

In order to map the applicability of each method, the models are applied on two different enthalpies, namely h $= 2900$kJ/kg and h $= 3600$kJ/kg. For each enthalpy, the results are shown for a range of wellhead pressures; $10-150$bar. These values are selected with the goals of the IDDP in mind; to access geofluid at subcritical pressures with temperatures up to $600°C$ (geofluid at h $= 3600$kJ/kg and p $= 150$bar has T $= 607°$C).

Many parameters, such as specific power, utilization efficiency, and condenser duty are recorded for each instance. This gives an overall view of how the relative applicability of the methods changes.

4 Results

In this section, the results for each individual model are presented. First, results are shown for a geofluid with $h = 2900 kJ/kg$, then for $h = 3600 kJ/kg$ and at last for the IDDP-1 conditions.

While this section displays results for individual models, the next section, Discussions, will compare them and comment on the difference.

The results from the model of a single-flash cycle with wet scrubbing were verified by comparing them to a model that Mannvit Engineering, an engineering consulting company, had made. The results from the two different models where almost identical, which supports the assumptions made in this study.

4.1 Dry Steam Cycle without Corrosion Mitigation

States of the geofluid, that are of interest, are shown in Figure 21 for a geofluid with $h = 2900 kJ/kg$ at $p_{wellhead} = 10 bar$ and $p_{wellhead} = 150 bar$, and $h = 3600 kJ/kg$ at the same wellhead pressures. The figure shows the highest and lowest wellhead pressure investigated for the two enthalpies that will be analyzed. It can be seen that superheat increases with enthalpy as well as pressure.

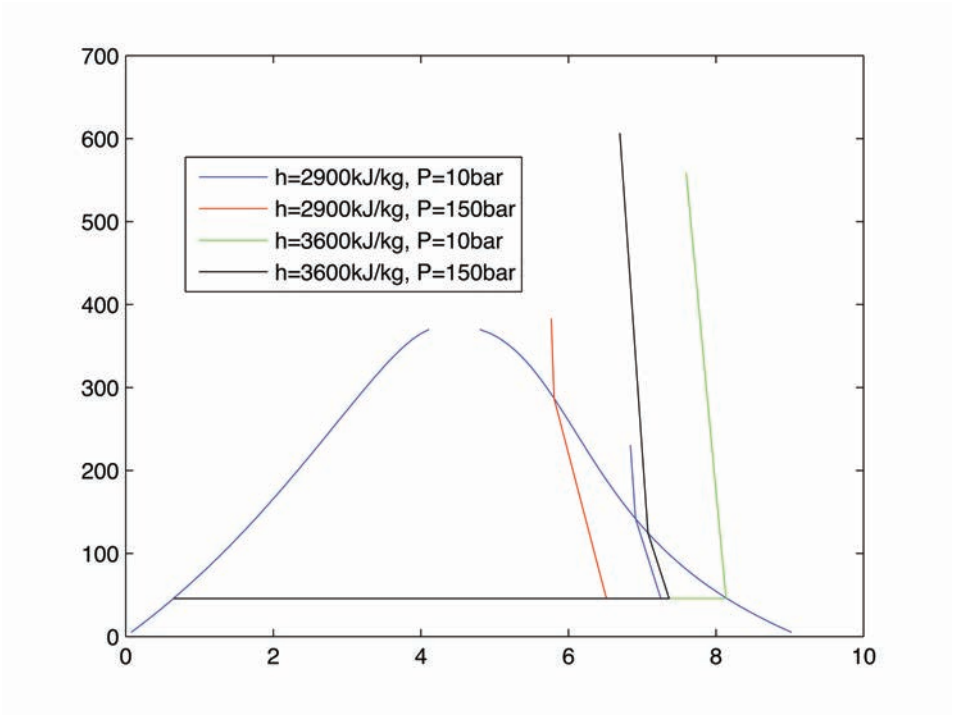

Figure 21: States that are of interest of geofluids with $h = 2900 kJ/kg$ at $p_{wellhead} = 10 bar$ and $p_{wellhead} = 150 bar$, and $h = 3600 kJ/kg$ at the same wellhead pressures.

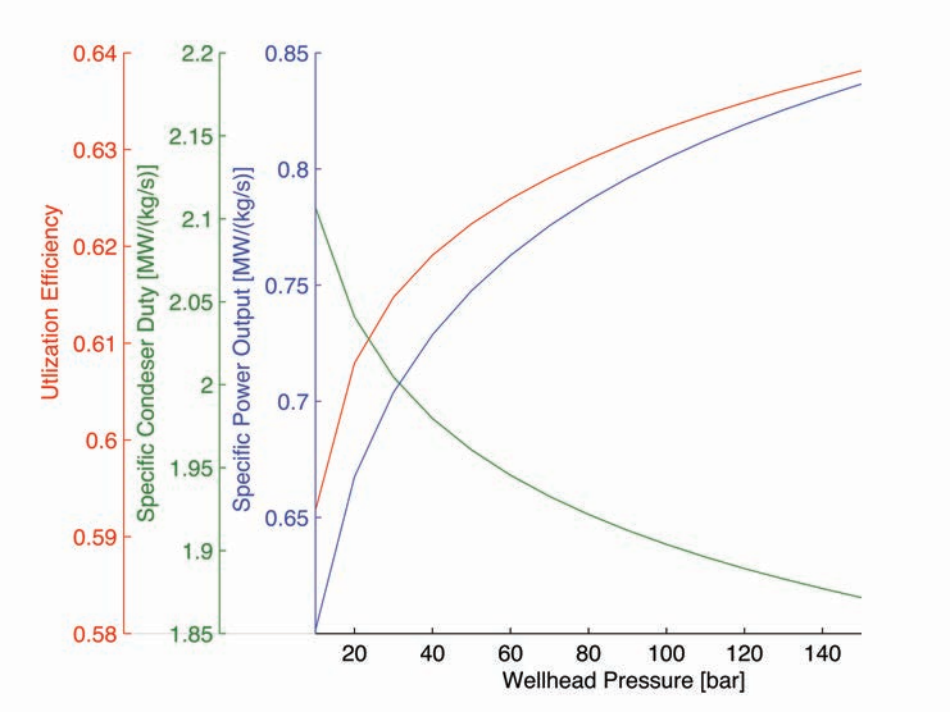

Figure 22: Properties of dry steam cycle working with a geofluid that has enthalpy of h = 2900kJ/kg. Each property is shown as a function of wellhead pressure. The color of each line corresponds to the color of its axis.

Figure 22 shows interesting properties of the power cycle for enthalpy of h = 2900kJ/kg at pressures ranging from 10 − 150bar. The figure shows how the specific net power increases with wellhead pressure. The reason is that at constant enthalpy, the superheat of the geofluid increases with the wellhead pressure. This can be seen in Figure 21, where the superheat of the geofluid is much greater when the pressure is 150bar than 10bar at the same enthalpy.

The same goes for the utilization efficiency, as shown in Figure 22, it increases with the wellhead pressure. Recalling that the efficiency of dry expansion in a turbine is higher than the one of wet expansion, it is easy to see that as the superheat increases, a larger portion of the expansion takes place with higher efficiency resulting in better total utilization efficiency.

Figure 22 also shows that the specific condenser duty decreases with increasing wellhead pressure. The reason is the increase in utilization efficiency. That is, less energy needs to be disposed because more is converted to electrical energy.

Figure 23 shows interesting properties of the power cycle for enthalpy of h = 3600kJ/kg at pressures ranging from 10 − 150bar. The relation between properties and wellhead pressure is similar to the one shown in Figure 22 for h = 2900kJ/kg.

Comparing figures 22 and 23, it can be seen that a higher enthalpy leads to higher net specific power output. This is not surprising, for enthalpy is a measure of the total energy

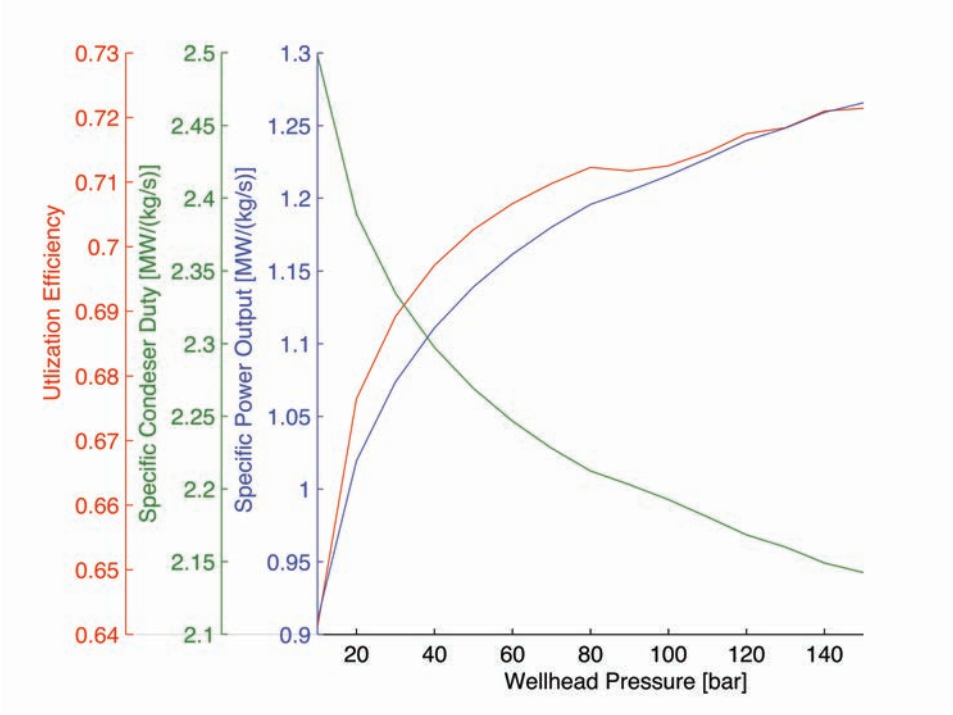

Figure 23: Properties of dry steam cycle working with a geofluid that has enthalpy of h = 3600kJ/kg. Each property is shown as a function of wellhead pressure. The color of each line corresponds to the color of its axis.

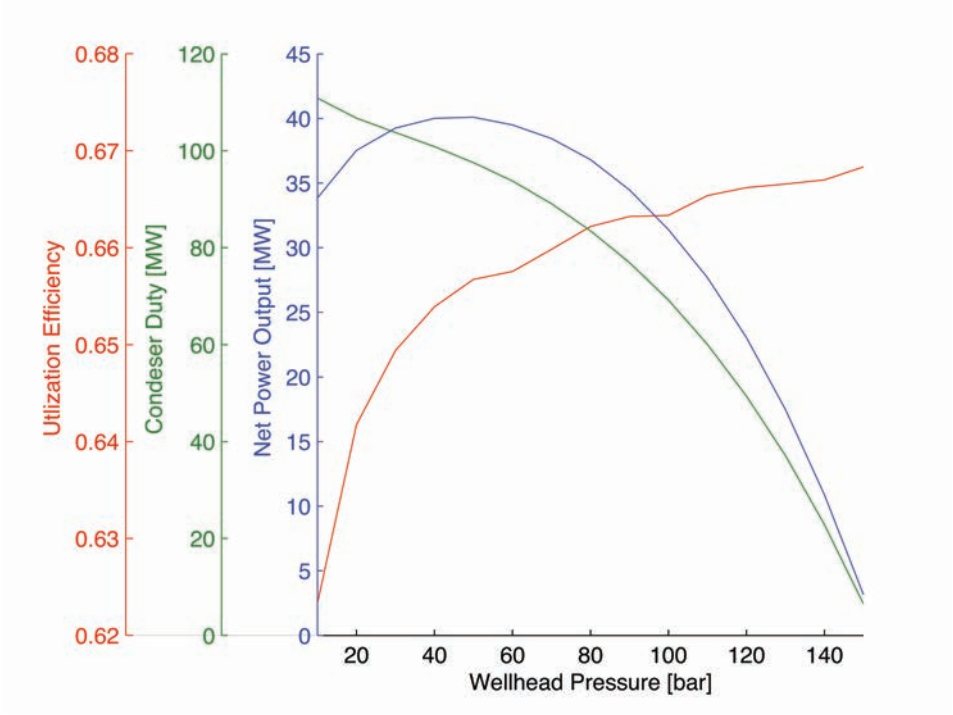

Figure 24: Properties of dry steam cycle working with a geofluid that has enthalpy of h = 3100kJ/kg, (similar to IDDP-1). Each property is shown as a function of wellhead pressure. The color of each line corresponds to the color of its axis.

Table 1: Results from economic analysis of dry steam cycle without corrosion mitigation

Case	Net Power [MW]	Overnight Capital Cost [$\$10^6$]	Monthly O$M Cost [$\$ * 10^3$]	Cost per kW [$\$/kW$]
IDDP-1	40.1	99	130	2500
h=2900kJ/kg	50.0	130	160	2500
h=3600kJ/kg	50.0	130	160	2500

content of the fluid. Also, superheat increases proportionally to enthalpy of a fluid at constant pressure, and as stated above, the total turbine efficiency increases with superheat. Note that the exergy of the geofluid increases as the enthalpy increases, see equation 33. So, a geofluid with higher exergy and a process with higher utilization efficiency results in more net power output.

In the same two figures, it can also be seen that the specific power increases with wellhead pressure. Although a larger fraction of the turbine expansion is wet expansion, resulting in a lower turbine efficiency, the exergy increases with pressure, due to lower entropy, increases the specific power output. The entropy can be seen in figure 21, and its relation to exergy in equation 33.

Figure 23 also shows that the specific condenser duty decreases with increasing wellhead pressure. Again, the reason is the increase in utilization efficiency.

The mass flow rate for IDDP-1, shown in Figure 20, is used to find the net power output if the dry steam power cycle would be applied on the borehole. This, along with other properties, is shown in Figure 24. It can be seen that the highest power output, 40.1MW, is obtained by using a wellhead pressure of 50bar. This clearly shows the tremendous potential of the IDDP; a conventional well produces about 8 times less power, or 5MW [21].

Although the utilization efficiency is not at its highest level, the decrease in mass flow rate at higher pressure makes for this shift in optimum pressure.

Figure 24 also shows that the condenser duty decreases with increasing wellhead pressure. The reason is the decrease in mass flow rate; less hot water to cool down.

The results from the exergy analysis are shown in a Grassmann diagram in figure 25. All arrows pointing upward show the amount of exergy *lost* in each process. While the arrow pointing rightward shows the electrical production.

Table 1 shows results from economic analysis carried out for the power cycle. The reason for the similarity between the cases with different enthalpies is because of the presumptions stated in section 3.3.

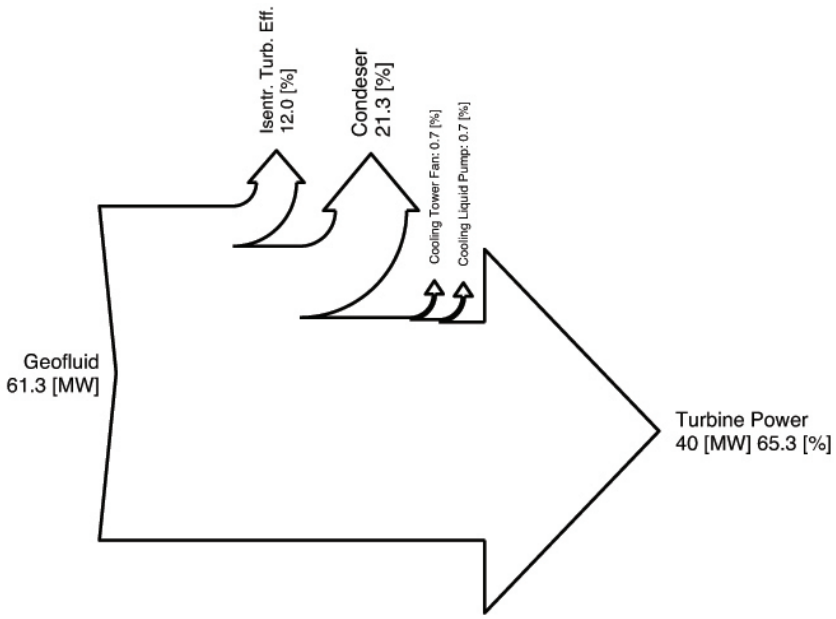

Figure 25: Results from exergy analysis for a dry steam cycle without corrosion mitigation. The Grassmann diagram shows the amount of exergy lost in each process in the power cycle.

4.2 Single-Flash Cycle with Wet Scrubbing

States of the geofluid, that are of interest, are shown in Figure 26 for a geofluid with $h = 2900\text{kJ/kg}$ at $p_{\text{wellhead}} = 10\text{bar}$ and $p_{\text{wellhead}} = 150\text{bar}$, and $h = 3600\text{kJ/kg}$ at the same wellhead pressures. The figure shows the thermodynamical process for the marginal cases in this study. It shows the highest and lowest wellhead pressure investigated for the two enthalpies that will be analyzed. It can be seen that superheat increases with enthalpy as well as pressure.

Figure 27 shows interesting properties of the power cycle for enthalpy of $h = 2900\text{kJ/kg}$ at pressures ranging from $10 - 150\text{bar}$. The figure shows how the specific net power increases with wellhead pressure. The reason is that at constant enthalpy, the superheat of the geofluid increases with the wellhead pressure. This can be seen in Figure 26, where the superheat of the geofluid is much greater when the pressure is 150bar than 10bar at constant enthalpy.

The utilization efficiency increases with wellhead pressure up to 80bar then it decreases again, as shown in Figure 27. As said above, the exergy of the fluid increases with wellhead pressure. The reason for this decrease in utilization efficiency at higher pressures is the larger fraction of the turbine expansion that takes place in the wet region, resulting in a lower turbine efficiency. So as the exergy of the geofluid increases, the specific net power output stays similar due to lower turbine efficiency, resulting in a lower utilization efficiency.

Figure 27 also shows that the specific condenser duty decreases with increasing wellhead

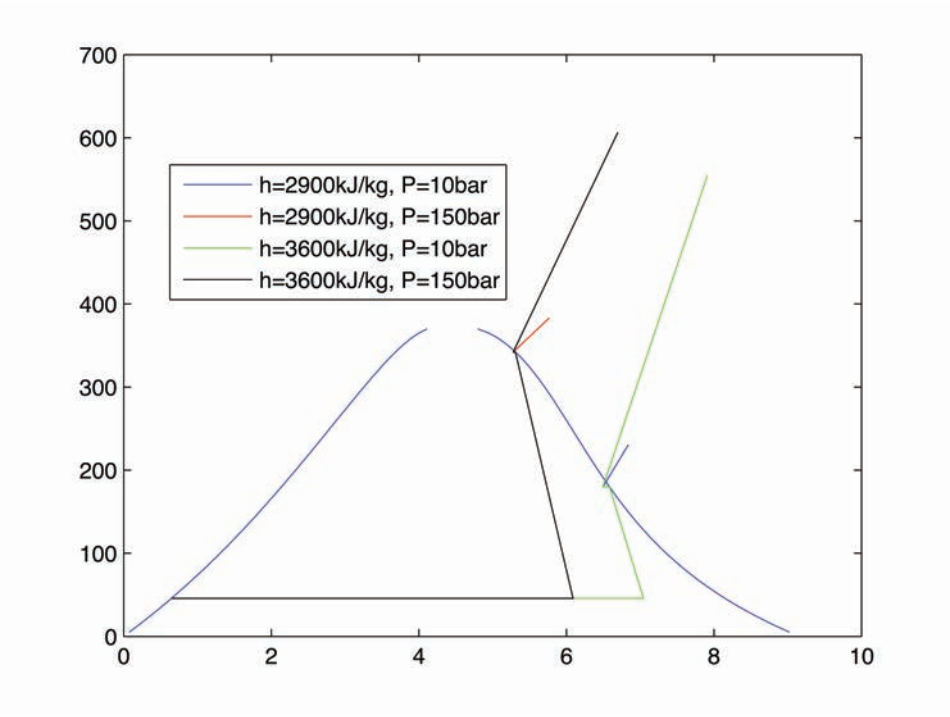

Figure 26: States that are of interest of geofluids with $h = 2900\text{kJ/kg}$ at $p_{\text{wellhead}} = 10\text{bar}$ and $p_{\text{wellhead}} = 150\text{bar}$, and $h = 3600\text{kJ/kg}$ at the same wellhead pressures.

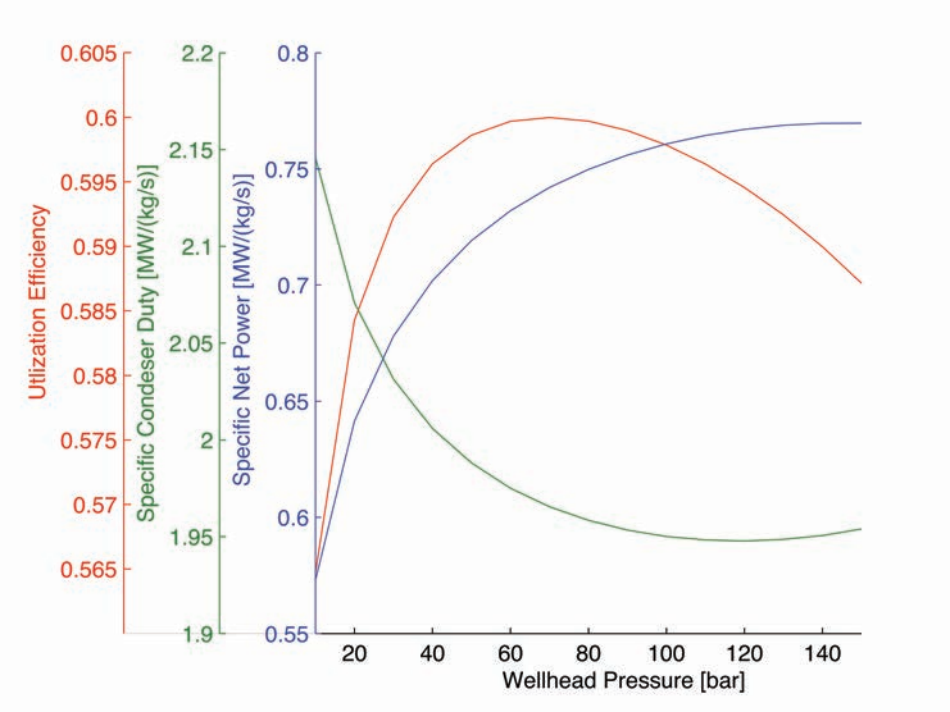

Figure 27: Properties of single-flash cycle with wet scrubbing working with a geofluid that has enthalpy of $h = 2900 kJ/kg$. Each property is shown as a function of wellhead pressure. The color of each line corresponds to the color of its axis.

pressure. The reason is the increase in utilization efficiency. That is, less energy needs to be disposed because more is converted to electrical energy. Note that as the utilization efficiency decreases again at higher pressures, the condenser duty increases.

Figure 28 shows interesting properties of the power cycle for enthalpy of $h = 3600 kJ/kg$ at pressures ranging from $10 - 150 bar$. The relation between properties and wellhead pressure is similar to the one shown in Figure 27 for $h = 2900 kJ/kg$.

Comparing figures 27 and 28, it can be seen that a higher enthalpy leads to higher net specific power output. The amount of injection water required to cool the steam below the saturated vapor curve increases proportionally to enthalpy, resulting in more mass flow rate. This is not surprising, for the quantity of liquid at $T < T_{geofluid}$ required to cool the geofluid increases with the geofluids' energy content. Note that the specific net power is given with respect to mass flow rate of geofluid. That is, amount of power per unit mass flow rate of geofluid, not essentially the total mass flow rate though the turbine.

In the same two figures, it can also be seen that the specific power increases with wellhead pressure. Although a larger fraction of the turbine expansion is wet expansion, resulting in a lower turbine efficiency, the exergy increases with pressure, due to lower entropy, increases the specific power output. The entropy can be seen in figure 26, and its relation to exergy in

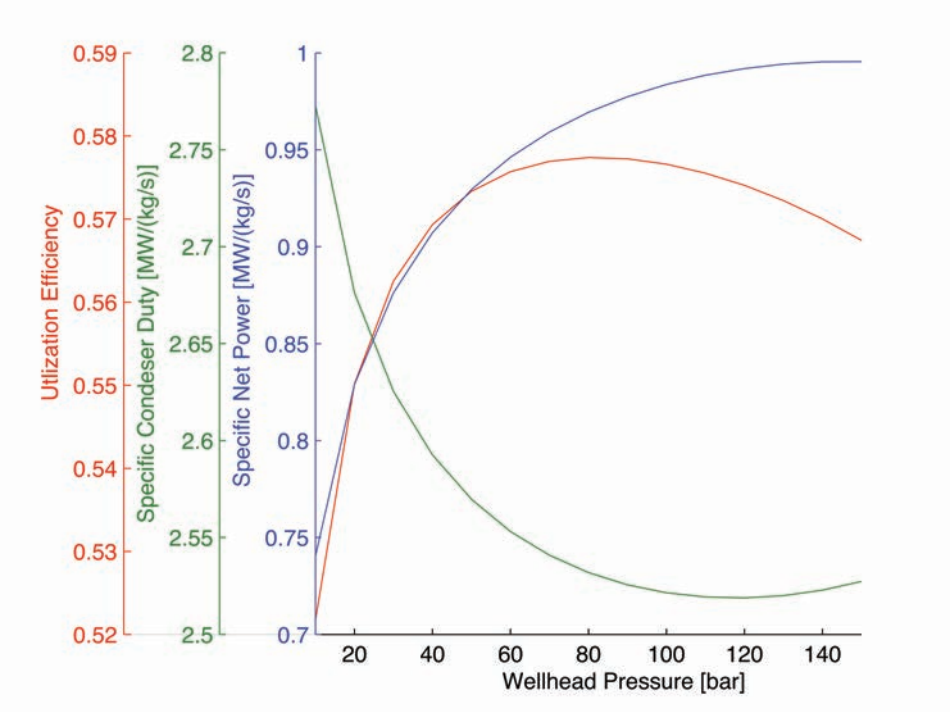

Figure 28: Properties of single-flash cycle with wet scrubbing working with a geofluid that has enthalpy of $h = 3600 kJ/kg$. Each property is shown as a function of wellhead pressure. The color of each line corresponds to the color of its axis.

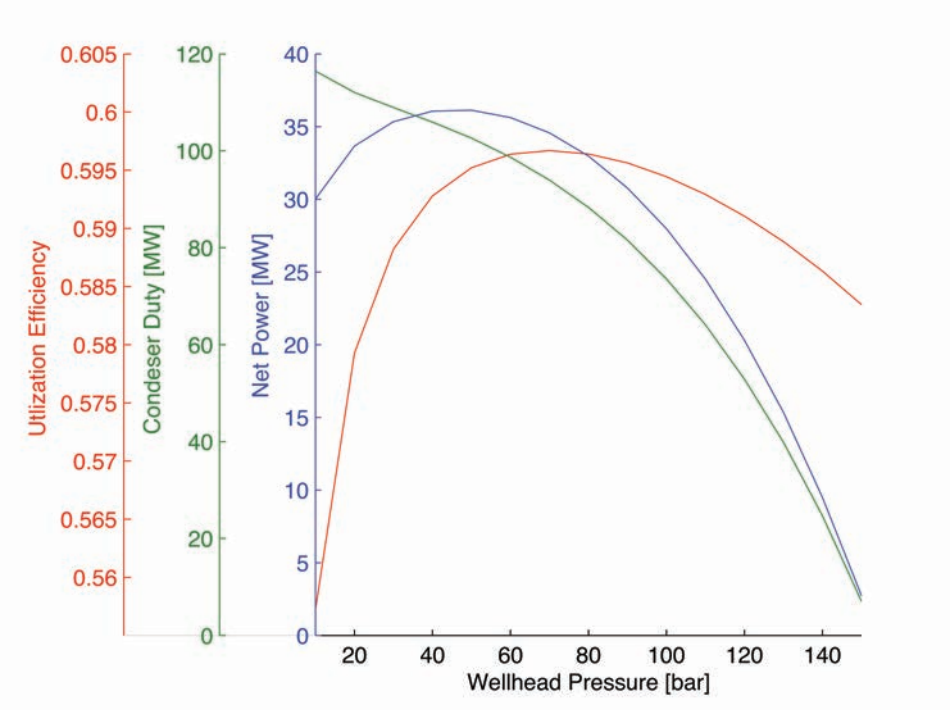

Figure 29: Properties of single-flash cycle with wet scrubbing working with a geofluid that has enthalpy of $h = 3100 kJ/kg$, (similar to IDDP-1). Each property is shown as a function of wellhead pressure. The color of each line corresponds to the color of its axis.

equation 33. Figure 28 also shows that the specific condenser duty decreases with increasing wellhead pressure and opposite. Again, the reason is the utilization efficiency.

The mass flow rate for IDDP-1, shown in Figure 20, is used to find the net power output from the power cycle. This, along with other properties, is shown in Figure 29. It can be seen that the highest power output, 36.1MW, is obtained by using a wellhead pressure at 50bar. Although the utilization efficiency is not at its highest level, the decrease in mass flow rate of geofluid at higher pressure causes this shift in optimum pressure.

Figure 29 also shows that the condenser duty decreases with increasing wellhead pressure. The reason is the decrease in mass flow rate; less hot water to cool down.

The results from the exergy analysis are shown by a Grassmann diagram in figure 30.

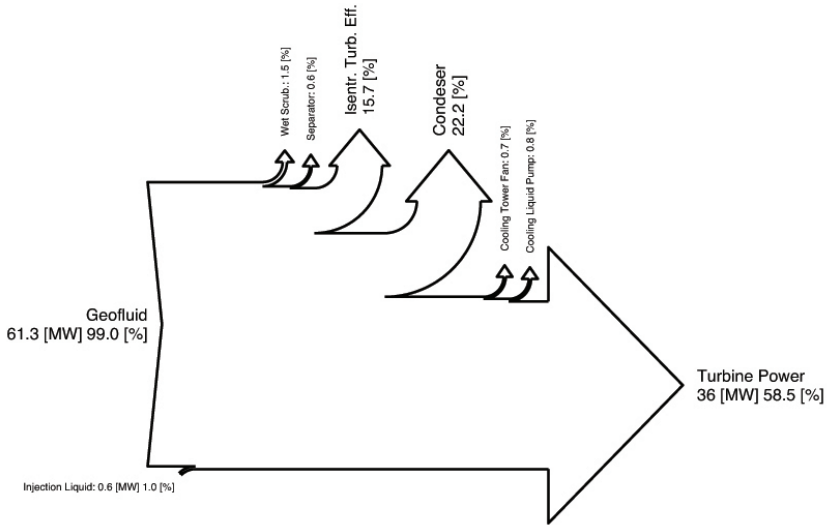

Figure 30: Results from exergy analysis for a single flash cycle with wet scrubbing. The Grassmann diagram shows the amount of exergy lost in each process in the power cycle.

Tables 2 and 3 show results for economic analysis carried out for the power cycle. The changes in the latter table, columns 2, 3, and 5, are with reference to dry steam cycle without corrosion mitigation. Using the presumptions stated in section 3.3, the overnight capital cost does not change significantly with enthalpy. It can be seen that change in cost per kW increases with enthalpy.

Table 2: Results from economic analysis of single flash cycle with wet scrubbing

Case	Net Power [MW]	Cost of Corrosion Mitigation System [$\$ * 10^6$]	Overnight Capital Cost [$\$10^6$]	Monthly O$M Cost [$\$ * 10^3$]
IDDP-1	36.1	0.20	95	130
h=2900kJ/kg	48.1	0.20	120	170
h=3600kJ/kg	40.7	0.20	120	150

Table 3: Additional results from economic analysis of single flash cycle with wet scrubbing

Case	Change in Overnight Capital Cost [$\$ * 10^6$]	Change in Power [MW]	Cost per kW [$\$/kW$]	Change in Cost per kW [$kW]
IDDP-1	-3.8	-3.9	2700	200
h=2900kJ/kg	-1.7	-1.9	2600	100
h=3600kJ/kg	-9.6	-9.3	2800	300

4.3 Single-Flash Cycle with Wet Scrubbing and Heat Recovery

States of the geofluid, that are of interest, are shown in Figure 31 for a geofluid with $h = 2900\text{kJ/kg}$ at $p_{\text{wellhead}} = 10\text{bar}$ and $p_{\text{wellhead}} = 150\text{bar}$, and $h = 3600\text{kJ/kg}$ at the same wellhead pressures. The figure shows the thermodynamical process for the marginal cases in this study. It shows the highest and lowest wellhead pressure investigated for the two enthalpies that will be analyzed. It can be seen that superheat increases with enthalpy as well as pressure. This will be referred to later on.

Figure 32 shows interesting properties of the power cycle for enthalpy of $h = 2900\text{kJ/kg}$ at pressures ranging from $10 - 150\text{bar}$. The figure shows how the specific net power increases with wellhead pressure. The reason is that at constant enthalpy, the superheat of the geofluid increases with the wellhead pressure. This can be seen in Figure 31, where the superheat of the geofluid is much greater when the pressure is 150bar than 10bar at constant enthalpy.

The utilization efficiency increases with wellhead pressure up to around 120bar then it decreases again, as it did for single flash power cycle with wet scrubbing. When compared to Figure 27 it is interesting to see how the heat recovery has decreased this down swing and shifted it to higher pressures.

Figure 32 also shows that the specific condenser duty decreases with increasing wellhead pressure, which happens for the same reasons as described above. Note that the condenser duty

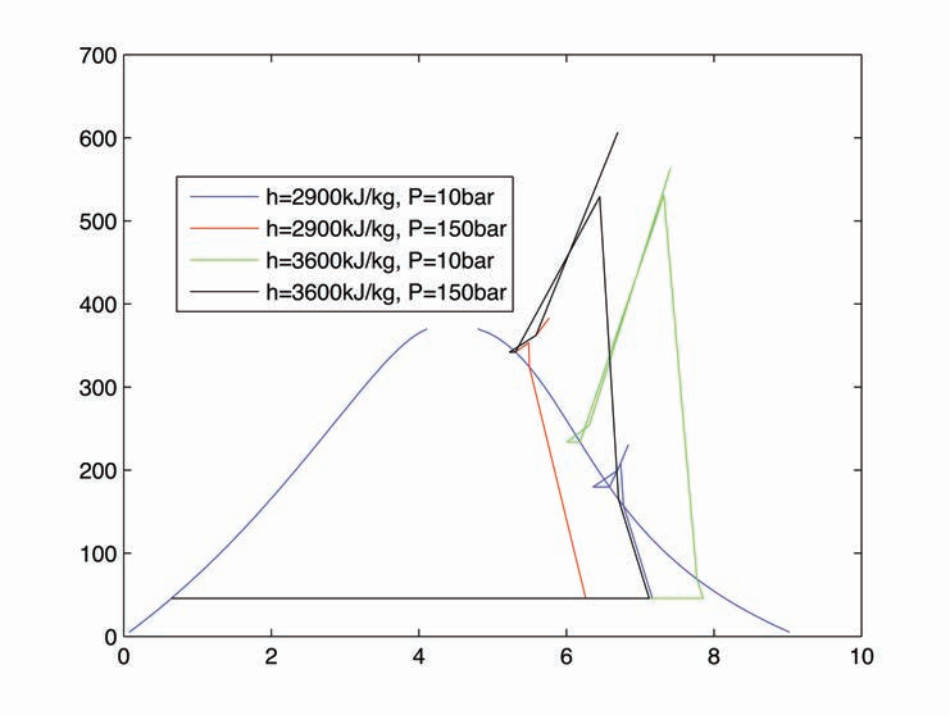

Figure 31: States that are of interest of geofluids with $h = 2900\text{kJ/kg}$ at $p_{\text{wellhead}} = 10\text{bar}$ and $p_{\text{wellhead}} = 150\text{bar}$, and $h = 3600\text{kJ/kg}$ at the same wellhead pressures.

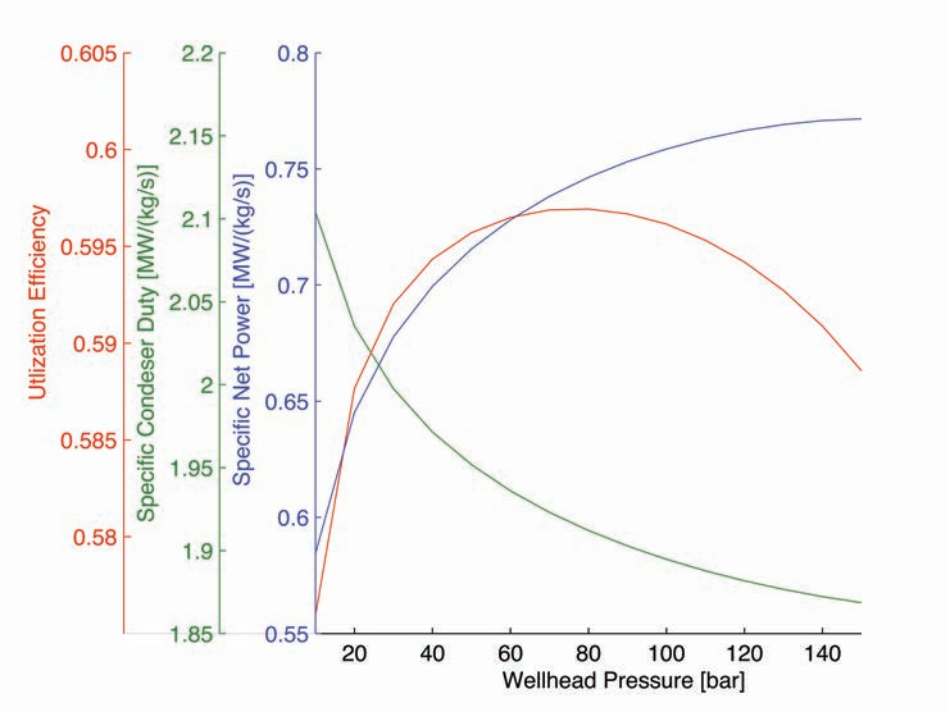

Figure 32: Properties of single-flash cycle with wet scrubbing and heat recovery working with a geofluid that has enthalpy of $h = 2900 kJ/kg$. Each property is shown as a function of wellhead pressure. The color of each line corresponds to the color of its axis.

does not increase again at higher pressure as it did for the single flash power cycle with wet scrubbing.

Figure 33 shows interesting properties of the power cycle working with geofluid with enthalpy of $h = 3600 kJ/kg$ at pressures ranging from $10 - 150$bar. The relation between properties and wellhead pressure is similar to the one shown in Figure 32 for $h = 2900 kJ/kg$.

Comparing figures 32 and 33, it can be seen that a higher enthalpy leads to higher net specific power output. In the same two figures, it can also be seen that the specific power increases with wellhead pressure. This happens for the same reasons as described above.

Figure 33 also shows that the specific condenser duty decreases with increasing wellhead pressure. Again, the reason is the relationship between utilization efficiency and condenser duty.

The mass flow rate for IDDP-1, shown in Figure 20, is used to find the net power output from the power cycle. This, along with other properties, is shown in Figure 34. It can be seen that the highest power output, 38.5MW, is obtained by using a wellhead pressure at 50bar.

The results from the exergy analysis are shown by a Grassmann diagram in figure 35.

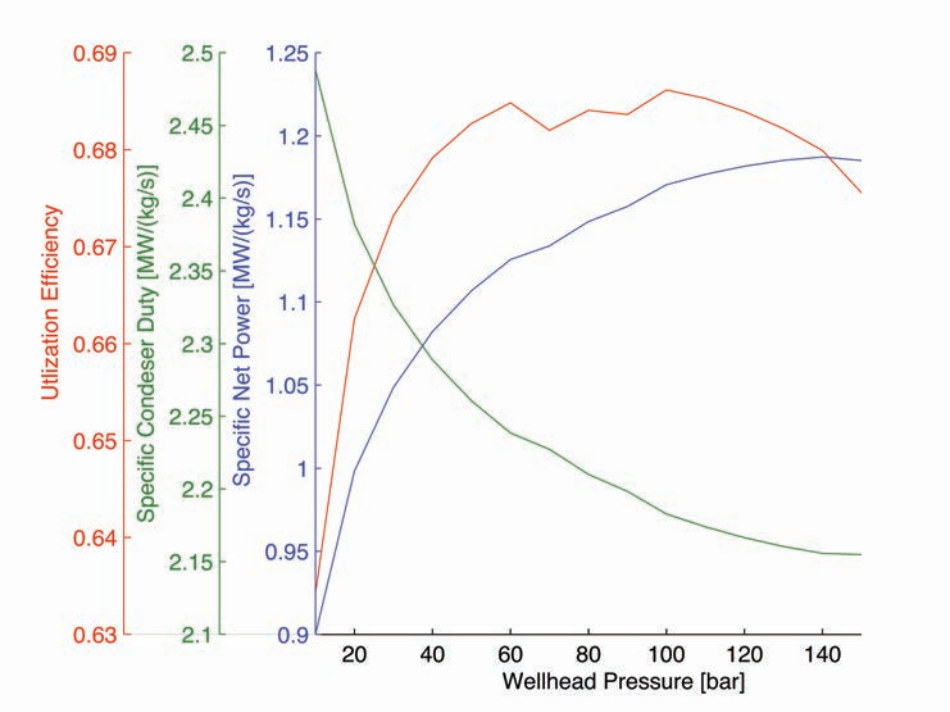

Figure 33: Properties of single-flash cycle with wet scrubbing with heat recovery working with a geofluid that has enthalpy of $h = 3600 kJ/kg$. Each property is shown as a function of wellhead pressure. The color of each line corresponds to the color of its axis.

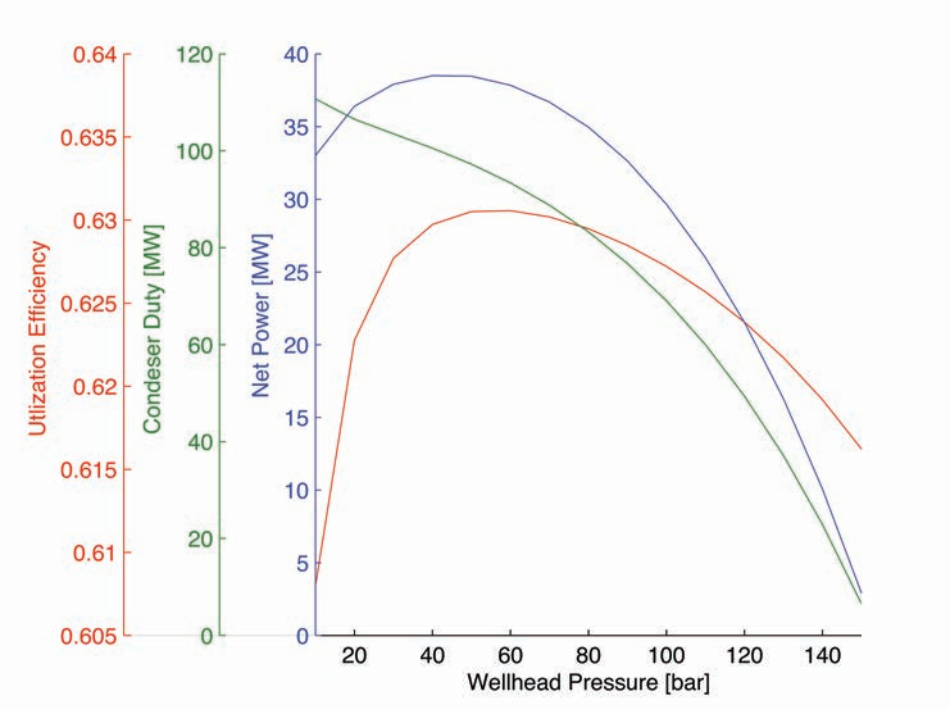

Figure 34: Properties of single-flash cycle with wet scrubbing and heat recovery working with a geofluid that has enthalpy of $h = 3100 kJ/kg$, (similar to IDDP-1). Each property is shown as a function of wellhead pressure. The color of each line corresponds to the color of its axis.

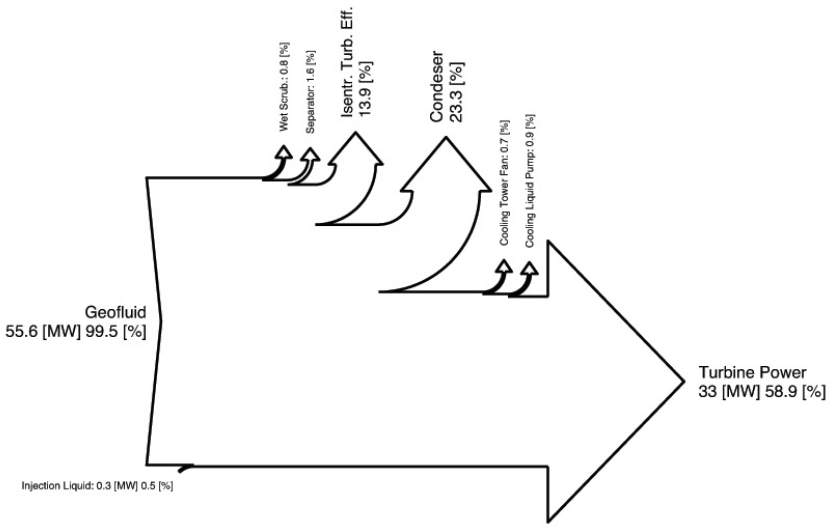

Figure 35: Results from exergy analysis for a single flash cycle with wet scrubbing with heat recovery. The Grassmann diagram shows the amount of exergy lost in each process in the power cycle.

Tables 4 and 5 show results for economic analysis carried out for the power cycle. The changes in the latter table columns 2, 3, and 5, are with reference to dry steam cycle without corrosion mitigation. Using the presumptions stated in section 3.3, the overnight capital cost changes with enthalpy, as can be seen for the cases of $\mathrm{h} = 2900\mathrm{kJ/kg}$ and $\mathrm{h} = 3600\mathrm{kJ/kg}$. It can be seen that change in cost per kW increases with enthalpy. The heat exchangers area used in the economic analysis was $5,000\mathrm{m}^2$ for the case of IDDP-1 but $1,100\mathrm{m}^2$ and $13,000\mathrm{m}^2$ for cases with $\mathrm{h} = 2900\mathrm{kJ/kg}$ and $\mathrm{h} = 3600\mathrm{kJ/kg}$, respectively.

Table 4: Results from economic analysis of single flash cycle with wet scrubbing and heat recovery

Case	Net Power [MW]	Cost of Corrosion Mitigation System [$\$ * 10^6$]	Overnight Capital Cost [$\$10^6$]	Monthly O$M Cost [$\$ * 10^3$]
IDDP-1	38.5	4.3	100	140
h=2900kJ/kg	47.9	1.4	120	170
h=3600kJ/kg	48.7	9.1	130	170

Table 5: Additional results from economic analysis of single flash cycle with wet scrubbing and heat recovery

Case	Change in Overnight Capital Cost [$\$ * 10^6$]	Change in Power [MW]	Cost per kW [$\$/kW$]	Change in Cost per kW [$kW]
IDDP-1	2.6	-1.7	2700	200
h=2900kJ/kg	-0.76	-2.1	2600	100
h=3600kJ/kg	7.7	-1.3	2700	200

4.4 Single-Flash Cycle with Wet Scrubbing and an Additional Turbine

States of the geofluid, that are of interest, are shown in Figure 36 for a geofluid with $h = 2900\text{kJ/kg}$ at $p_{\text{wellhead}} = 10\text{bar}$ and $p_{\text{wellhead}} = 150\text{bar}$, and $h = 3600\text{kJ/kg}$ at the same wellhead pressures. The figure shows the thermodynamical process for the marginal cases in this study. It shows the highest and lowest wellhead pressure investigated for the two enthalpies that will be analyzed. It can be seen that superheat increases with enthalpy as well as pressure.

Figure 37 shows interesting properties of the power cycle for enthalpy of $h = 2900\text{kJ/kg}$ at pressures ranging from $10 - 150\text{bar}$. The figure shows how the specific net power increases with wellhead pressure. The reason is that at constant enthalpy, the superheat of the geofluid increases with the wellhead pressure. This can be seen in Figure 36, where the superheat of the geofluid is much greater when the pressure is 150bar than 10bar at constant enthalpy.

The utilization efficiency increases with wellhead pressure. Figure 37 also shows that the specific condenser duty decreases with increasing wellhead pressure. Note that again, the condenser duty does not increase again at higher pressure as it did for the single flash power cycle with wet scrubbing.

Figure 38 shows interesting properties of the power cycle working with geofluid with enthalpy of $h = 3600\text{kJ/kg}$ at pressures ranging from $10 - 150\text{bar}$. The relation between proper-

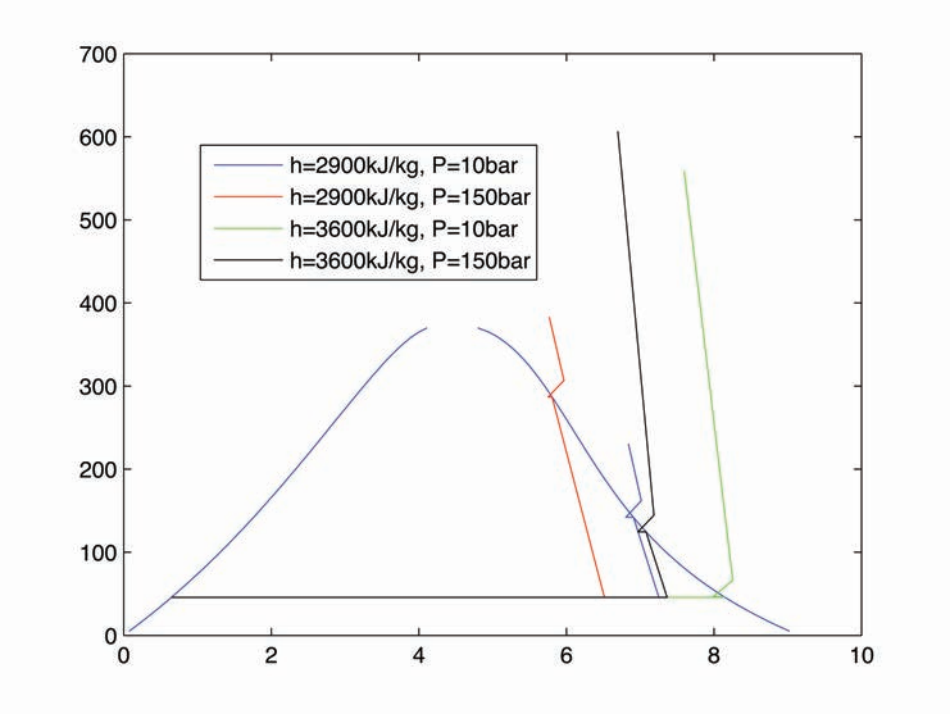

Figure 36: States that are of interest of geofluids with $h = 2900\text{kJ/kg}$ at $p_{\text{wellhead}} = 10\text{bar}$ and $p_{\text{wellhead}} = 150\text{bar}$, and $h = 3600\text{kJ/kg}$ at the same wellhead pressures.

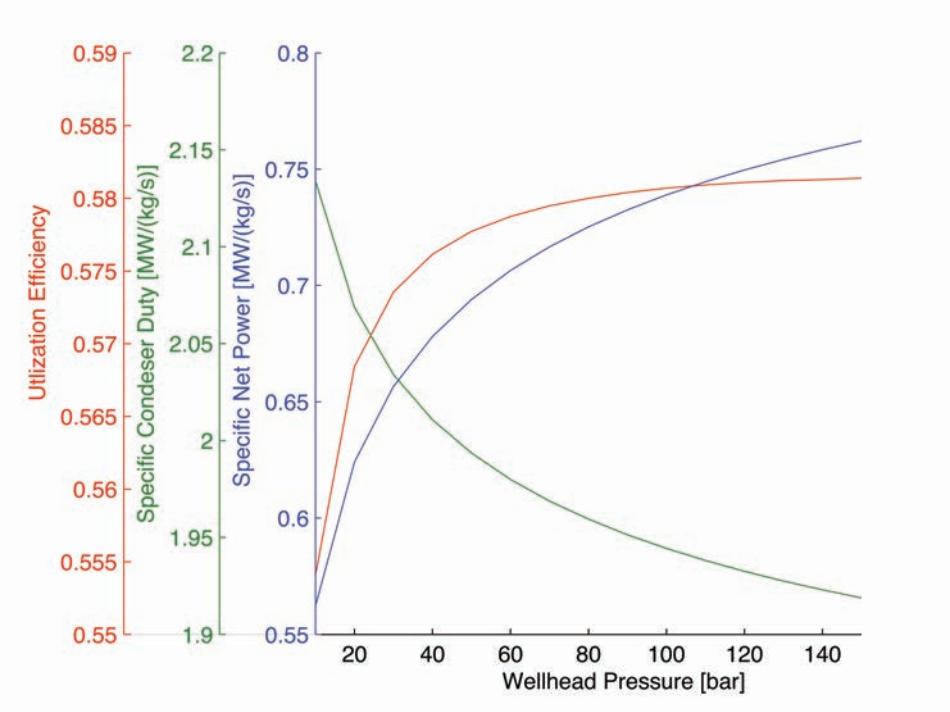

Figure 37: Properties of single-flash cycle with wet scrubbing and an additional turbine working with a geofluid that has enthalpy of $h = 2900 \mathrm{kJ/kg}$. Each property is shown as a function of wellhead pressure. The color of each line corresponds to the color of its axis.

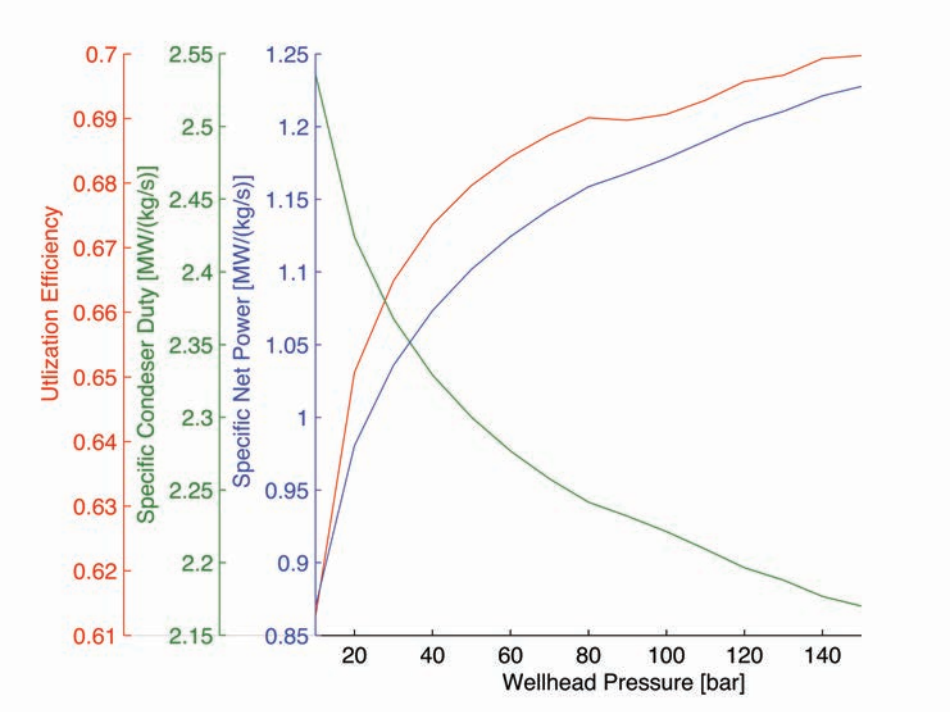

Figure 38: Properties of single-flash cycle with wet scrubbing and an additional turbine working with a geofluid that has enthalpy of $h = 3600 \mathrm{kJ/kg}$. Each property is shown as a function of wellhead pressure. The color of each line corresponds to the color of its axis.

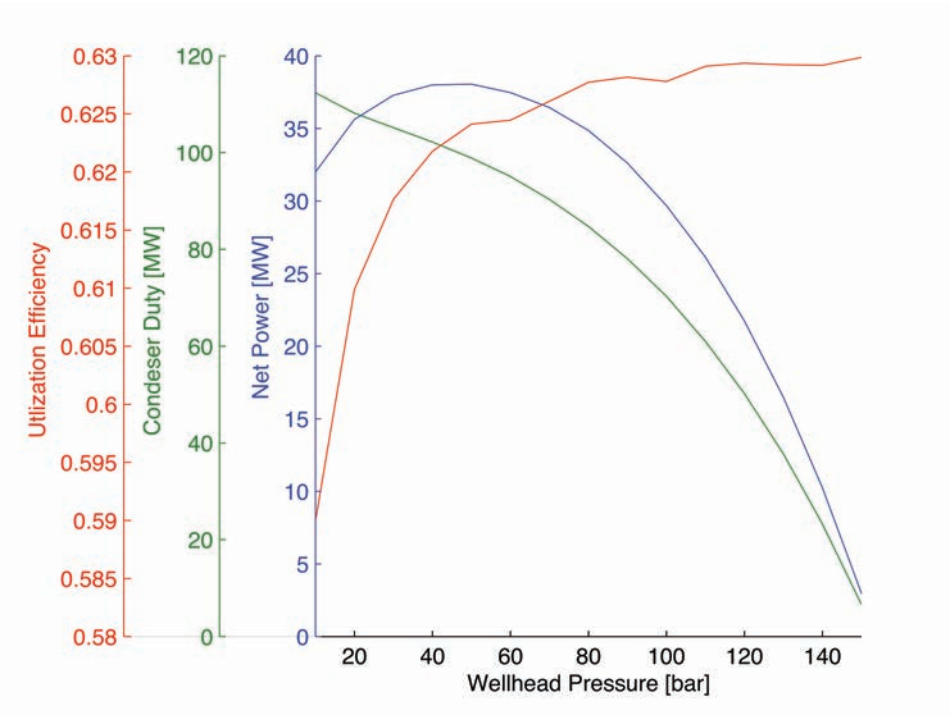

Figure 39: Properties of single-flash cycle with wet scrubbing and an additional turbine working with a geofluid that has enthalpy of h $= 3100$kJ/kg, (similar to IDDP-1). Each property is shown as a function of wellhead pressure. The color of each line corresponds to the color of its axis.

ties and wellhead pressure is similar to the one shown in Figure 37 for h $= 2900$kJ/kg.

Comparing figures 37 and 38, it can be seen that a higher enthalpy leads to higher net specific power output. In the same two figures, it can also be seen that the specific power increases with wellhead pressure. This is the same behavior as described above.

The mass flow rate for IDDP-1, shown in Figure 20, is used to find the net power output from the power cycle. This, along with other properties, is shown in Figure 39. It can be seen that the highest power output, 38.1MW, is obtained by using a wellhead pressure at 50bar.

The results from the exergy analysis are shown by a Grassmann diagram in figure 40.

Tables 6 and 7 show results for economic analysis carried out for the power cycle. The changes in the latter table columns 2, 3, and 5, are with reference to dry steam cycle without corrosion mitigation. Using the presumptions stated in section 3.3, the overnight capital cost changes significantly with enthalpy, as can be seen for the cases of h $= 2900$kJ/kg and h $=$ 3600kJ/kg. Also, the cost per kW increases with enthalpy.

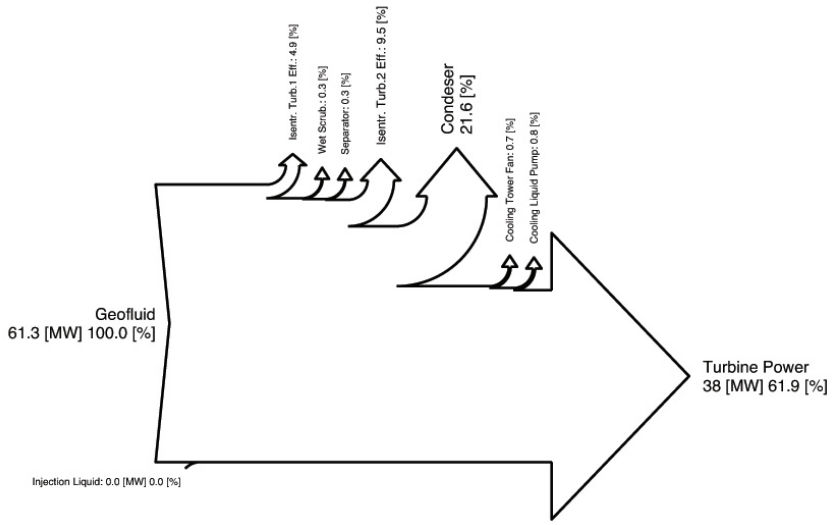

Figure 40: Results from exergy analysis for a single flash cycle with wet scrubbing with an additional turbine. The Grassmann diagram shows the amount of exergy lost in each process in the power cycle.

Table 6: Results from economic analysis of single flash cycle with wet scrubbing and an additional turbine

Case	Net Power [MW]	Cost of Corrosion Mitigation System [$\$ * 10^6$]	Overnight Capital Cost [$\$10^6$]	Monthly O\$M Cost [$\$ * 10^3$]
IDDP-1	38.1	5.8	100	130
h=2900kJ/kg	46.4	0.85	120	160
h=3600kJ/kg	48.2	16	140	170

Table 7: Additional results from economic analysis of single flash cycle with wet scrubbing and an additional turbine

Case	Change in Overnight Capital Cost [$\$ * 10^6$]	Change in Power [MW]	Cost per kW [$\$/kW$]	Change in Cost per kW [\$kW]
IDDP-1	3.6	-2.1	2700	200
h=2900kJ/kg	-2.8	-3.6	2600	100
h=3600kJ/kg	14	-1.8	2900	400

4.5 Dry Steam Cycle with Dry Steam Scrubbing

States of the geofluid, that are of interest, are shown in Figure 41 for a geofluid with $h = 2900\text{kJ/kg}$ at $p_{\text{wellhead}} = 10\text{bar}$ and $p_{\text{wellhead}} = 150\text{bar}$, and $h = 3600\text{kJ/kg}$ at the same wellhead pressures. The figure shows the thermodynamical process for the marginal cases in this study. It shows the highest and lowest wellhead pressure investigated for the two enthalpies that will be analyzed. It can be seen that superheat increases with enthalpy as well as pressure. This will be referred to later on.

Figure 42 shows interesting properties of the power cycle for enthalpy of $h = 2900\text{kJ/kg}$ at pressures ranging from $10 - 150\text{bar}$. The figure shows how the specific net power increases with wellhead pressure. The reason is that at constant enthalpy, the superheat of the geofluid increases with the wellhead pressure. This can be seen in Figure 41, where the superheat of the geofluid is much greater when the pressure is 150bar than 10bar at constant enthalpy.

The utilization efficiency increases with wellhead pressure. Figure 42 also shows that the specific condenser duty decreases with increasing wellhead pressure. This happens for the same reasons as described above.

Figure 43 shows interesting properties of the power cycle working with geofluid with enthalpy of $h = 3600\text{kJ/kg}$ at pressures ranging from $10 - 150\text{bar}$. The relation between proper-

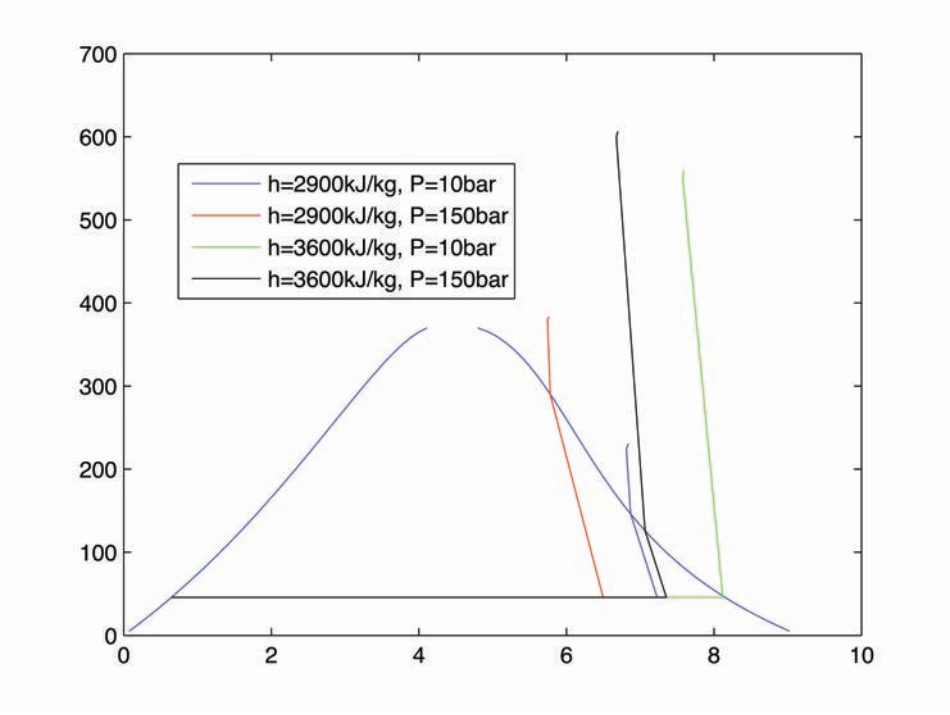

Figure 41: States that are of interest of geofluids with $h = 2900\text{kJ/kg}$ at $p_{\text{wellhead}} = 10\text{bar}$ and $p_{\text{wellhead}} = 150\text{bar}$, and $h = 3600\text{kJ/kg}$ at the same wellhead pressures.

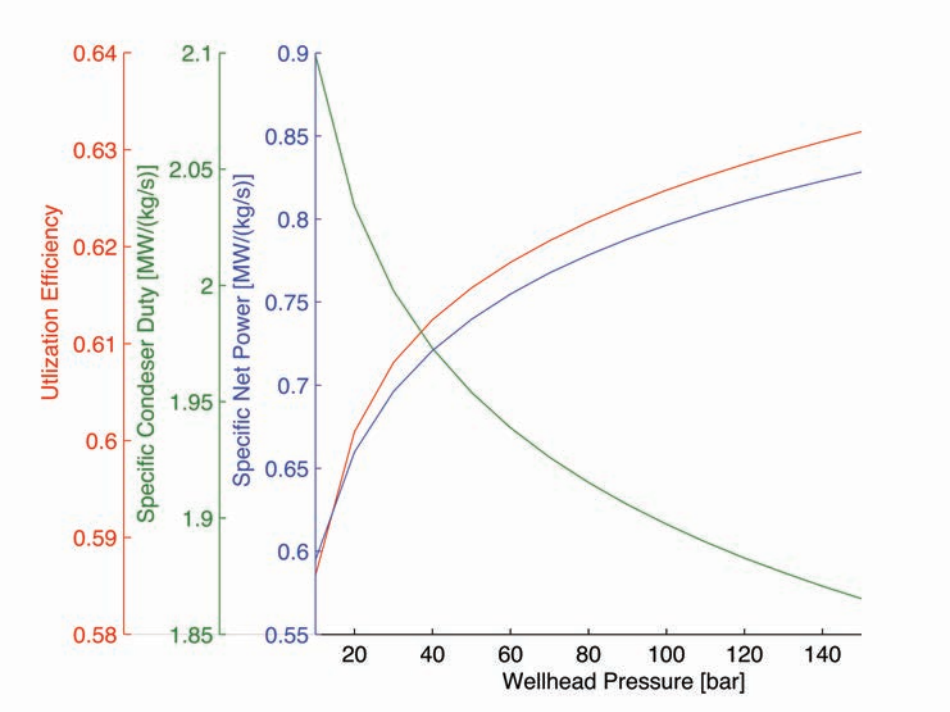

Figure 42: Properties of single-flash cycle with wet scrubbing and heat recovery working with a geofluid that has enthalpy of $h = 2900 kJ/kg$. Each property is shown as a function of wellhead pressure. The color of each line corresponds to the color of its axis.

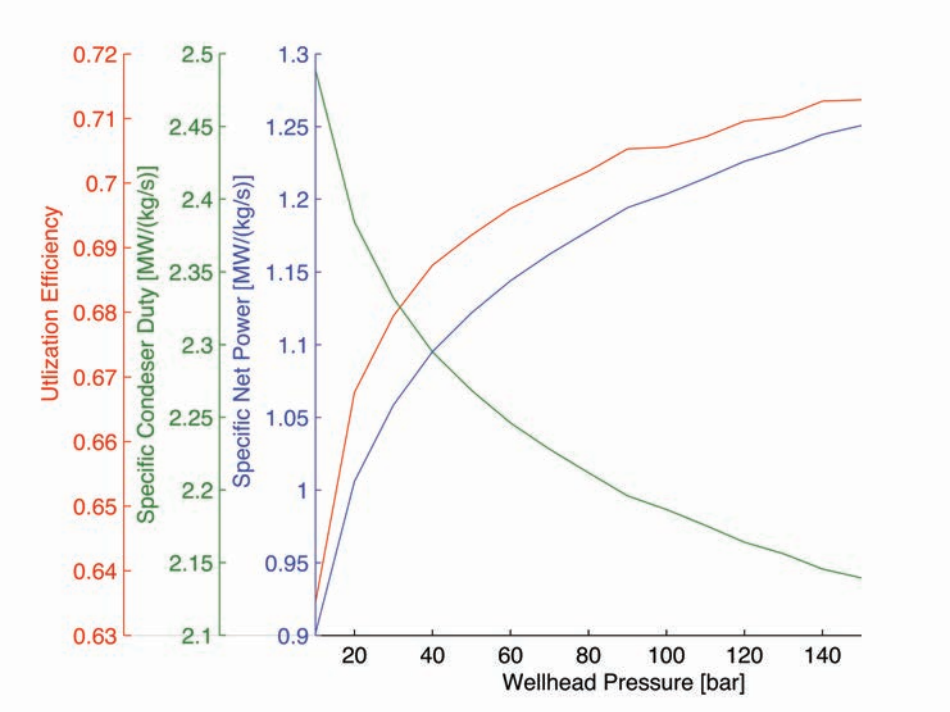

Figure 43: Properties of single-flash cycle with wet scrubbing with heat recovery working with a geofluid that has enthalpy of $h = 3600 kJ/kg$. Each property is shown as a function of wellhead pressure. The color of each line corresponds to the color of its axis.

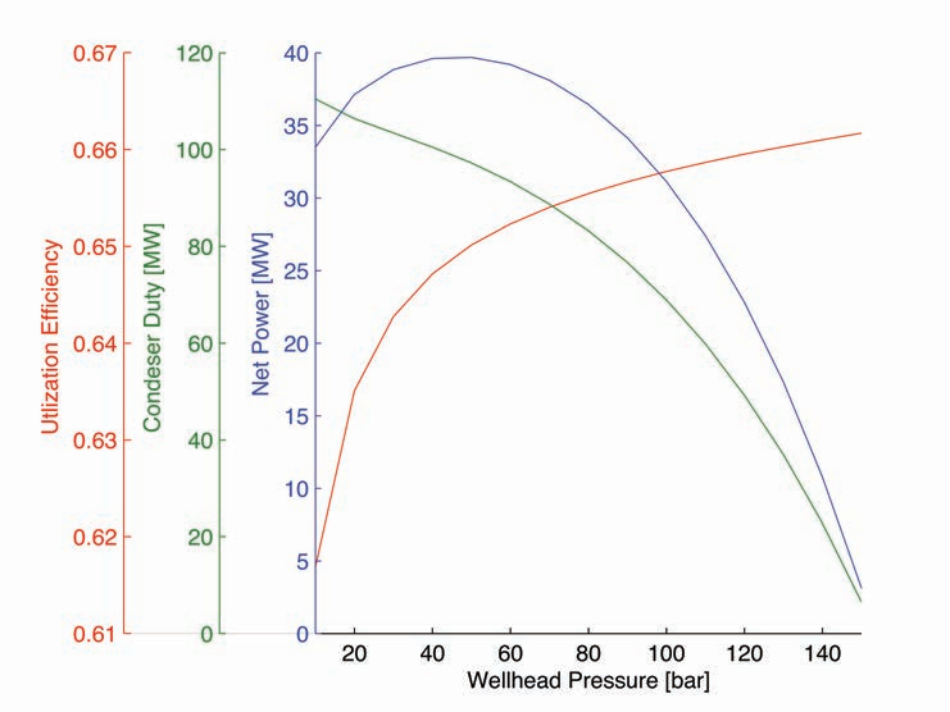

Figure 44: Properties of single-flash cycle with wet scrubbing working with a geofluid that has enthalpy of h $= 3100$kJ/kg, (similar to IDDP-1). Each property is shown as a function of wellhead pressure. The color of each line corresponds to the color of its axis.

ties and wellhead pressure is similar to the one shown in Figure 42 for h $= 2900$kJ/kg.

Comparing figures 42 and 43, it can be seen that a higher enthalpy leads to higher net specific power output. In the same two figures, it can also be seen that the specific power increases with wellhead pressure. Figure 43 also shows that the specific condenser duty decreases with increasing wellhead pressure. This behavior is explained in detail above.

The mass flow rate for IDDP-1, shown in Figure 20, is used to find the net power output from the power cycle. This, along with other properties, is shown in Figure 44. It can be seen that the highest power output, 39.7MW, is obtained by using a wellhead pressure at 50bar.

The results from the exergy analysis are shown by a Grassmann diagram in figure 45.

Tables 8 and 9 show results for economic analysis carried out for the power cycle. The changes in the latter table columns 2, 3, and 5, are with reference to dry steam cycle without corrosion mitigation. Using the presumptions stated in section 3.3, the overnight capital cost do not change with enthalpy, as can be seen for the cases of h $= 2900$kJ/kg and h $= 3600$kJ/kg. The cost per kW is the same for all enthalpies and does not vary significantly from dry steam cycle without corrosion mitigation.

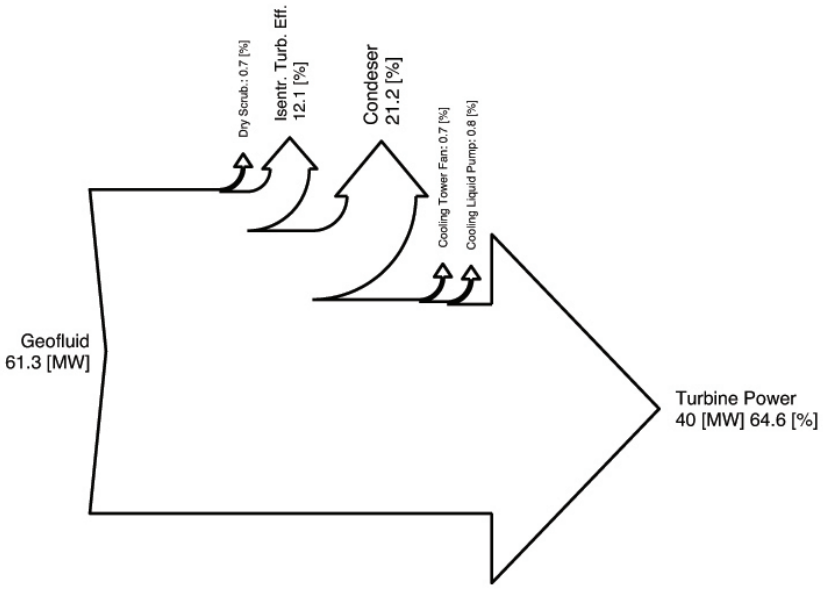

Figure 45: Results from exergy analysis for a dry steam cycle with dry scrubbing. The Grassmann diagram shows the amount of exergy lost in each process in the power cycle.

Table 8: Results from economic analysis of dry steam cycle with dry scrubbing

Case	Net Power [MW]	Cost of Corrosion Mitigation System [$\$ * 10^6$]	Overnight Capital Cost [$\$10^6$]	Monthly O$M Cost [$\$ * 10^3$]
IDDP-1	39.7	1.0	99	130
h=2900kJ/kg	49.5	1.0	130	170
h=3600kJ/kg	49.1	1.0	130	170

Table 9: Additional results from economic analysis of dry steam cycle with dry scrubbing

Case	Change in Overnight Capital Cost [$\$ * 10^6$]	Change in Power [MW]	Cost per kW [$\$/kW$]	Change in Cost per kW [$kW]
IDDP-1	0.50	-0.50	2500	0
h=2900kJ/kg	0.46	-0.54	2500	0
h=3600kJ/kg	0.12	-0.88	2500	0

4.6 Binary Cycle

States of the geofluid, that are of interest, are shown in Figure 46 for a geofluid with $h = 2900\text{kJ/kg}$ at $p_{wellhead} = 10\text{bar}$ and $p_{wellhead} = 150\text{bar}$, and $h = 3600\text{kJ/kg}$ at the same wellhead pressures. The figure shows the thermodynamical process for the marginal cases in this study. It shows the highest and lowest wellhead pressure investigated for the two enthalpies that will be analyzed. It can be seen that superheat increases with enthalpy as well as pressure.

Figure 47 shows interesting properties of the power cycle for enthalpy of $h = 2900\text{kJ/kg}$ at pressures ranging from $10 - 150\text{bar}$. The figure shows how the specific net power increases with wellhead pressure. The reason is that at constant enthalpy, the superheat of the geofluid increases with the wellhead pressure. This can be seen in Figure 46, where the superheat of the geofluid is much greater when the pressure is 150bar than 10bar at constant enthalpy.

The utilization efficiency increases with wellhead pressure. Figure 47 also shows that the specific condenser duty decreases with increasing wellhead pressure. This behavior is explained above.

Figure 48 shows interesting properties of the power cycle working with geofluid with enthalpy of $h = 3600\text{kJ/kg}$ at pressures ranging from $10 - 150\text{bar}$. The relation between properties and wellhead pressure is similar to the one shown in Figure 47 for $h = 2900\text{kJ/kg}$.

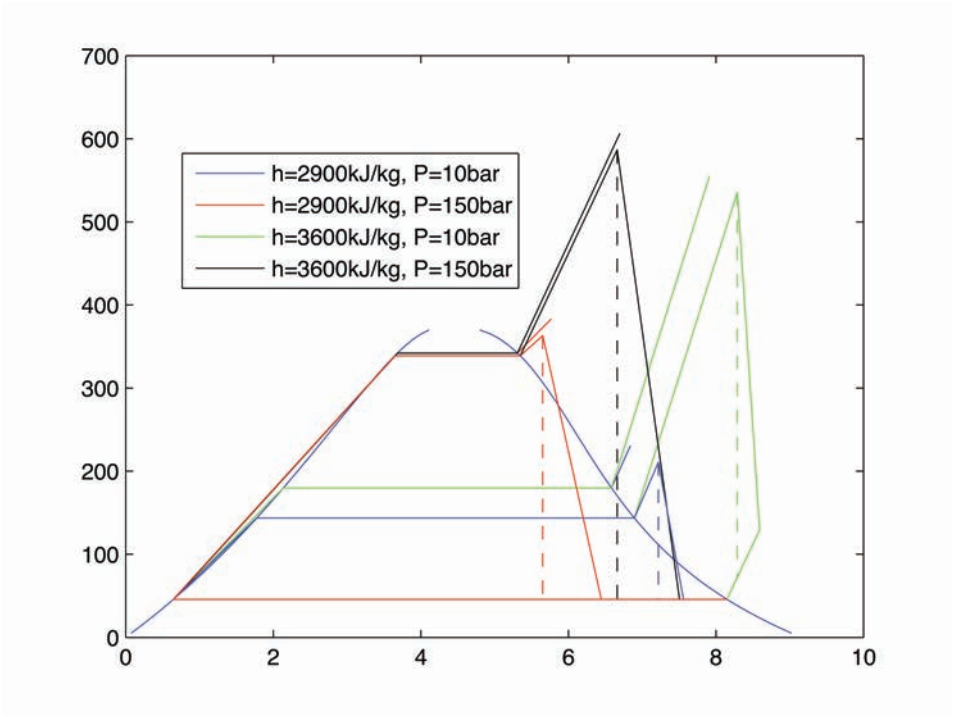

Figure 46: States that are of interest of geofluids with $h = 2900\text{kJ/kg}$ at $p_{wellhead} = 10\text{bar}$ and $p_{wellhead} = 150\text{bar}$, and $h = 3600\text{kJ/kg}$ at the same wellhead pressures.

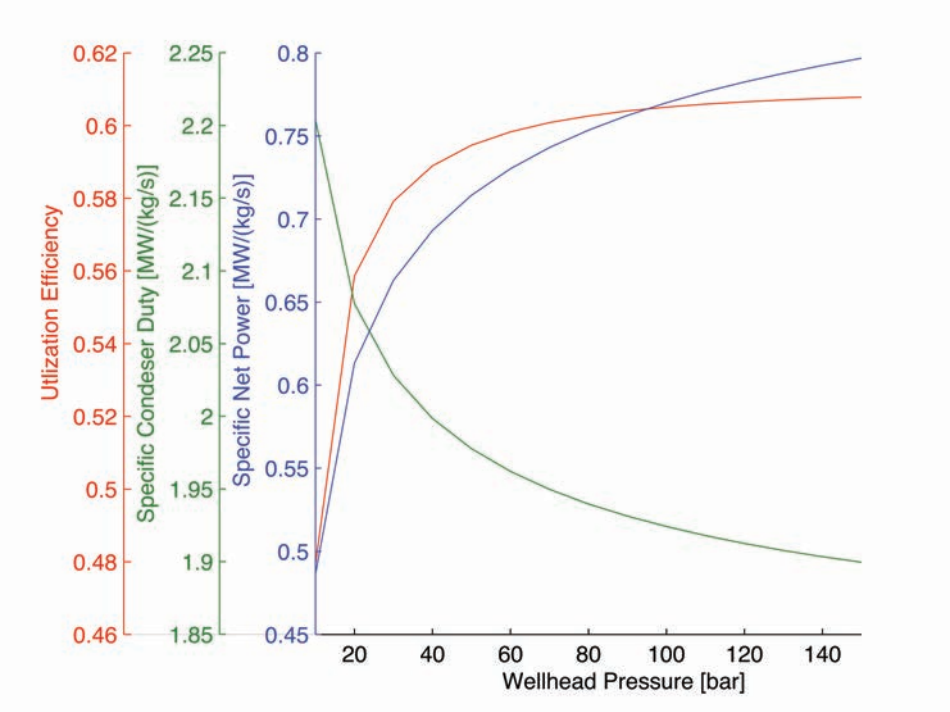

Figure 47: Properties of binary cycle with condensation in heat exchanger working with a geofluid that has enthalpy of $h = 2900 kJ/kg$. Each property is shown as a function of wellhead pressure. The color of each line corresponds to the color of its axis.

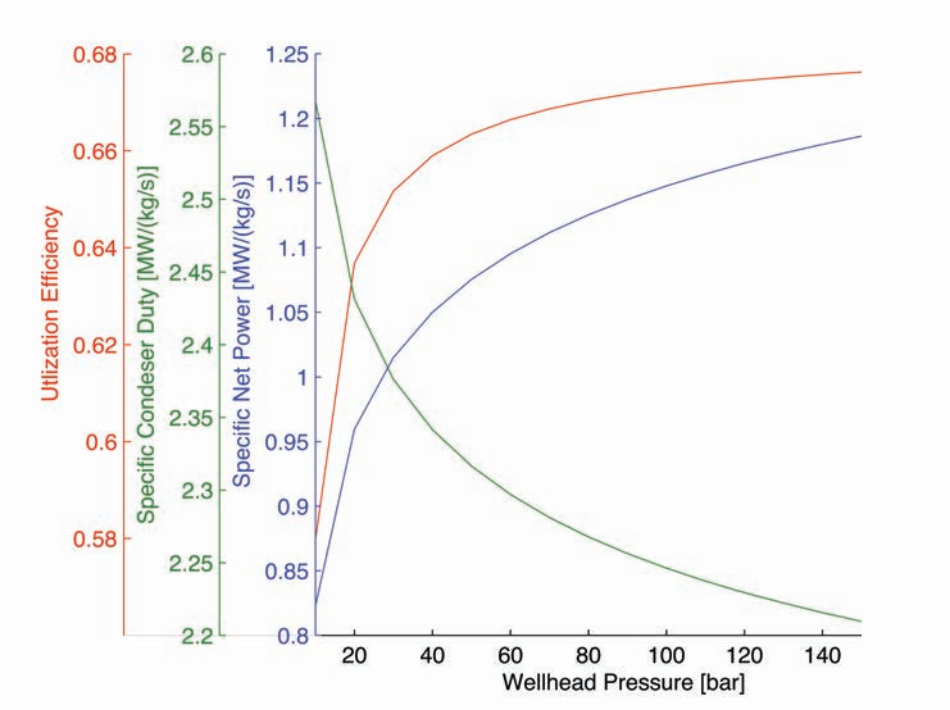

Figure 48: Properties of binary cycle with condensation in heat exchanger working with a geofluid that has enthalpy of $h = 3600 kJ/kg$. Each property is shown as a function of wellhead pressure. The color of each line corresponds to the color of its axis.

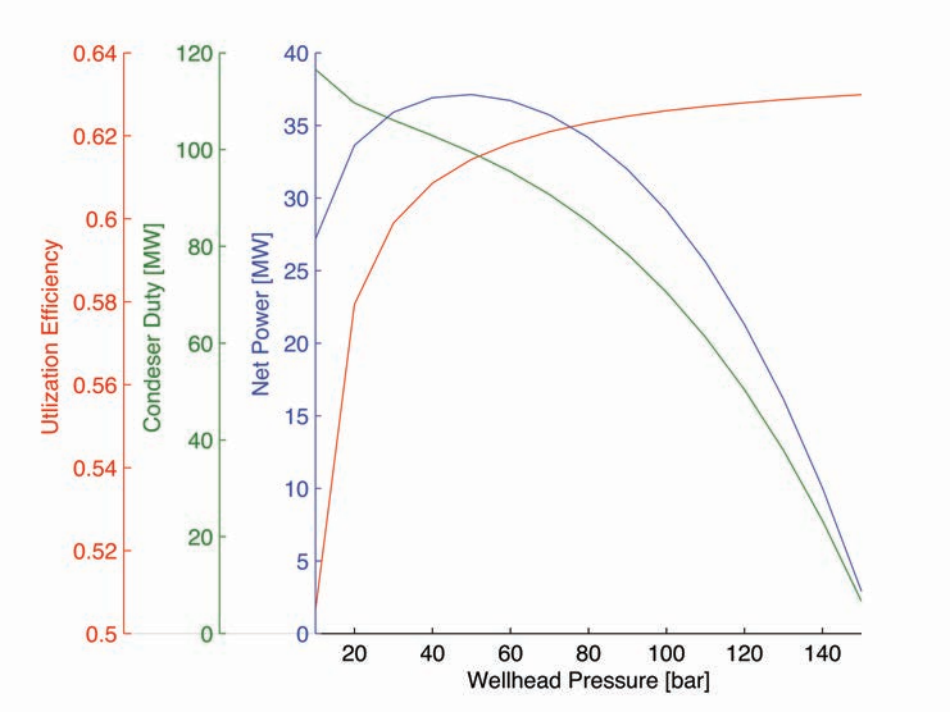

Figure 49: Properties of binary cycle with condensation in heat exchanger that has enthalpy of $h = 3100 kJ/kg$, (similar to IDDP-1). Each property is shown as a function of wellhead pressure. The color of each line corresponds to the color of its axis.

Comparing figures 47 and 28, it can be seen that a higher enthalpy leads to higher net specific power output. In the same two figures, it can also be seen that the specific power increases with wellhead pressure. Figure 48 also shows that the specific condenser duty decreases with increasing wellhead pressure. Again, this is the same behavior as explained earlier.

The mass flow rate for IDDP-1, shown in Figure 20, is used to find the net power output from the power cycle. This, along with other properties, is shown in Figure 49. It can be seen that the highest power output, 37.1MW, is obtained by using a wellhead pressure at 50bar.

The results from the exergy analysis are shown by a Grassmann diagram in figure 50.

Tables 10 and 11 show results for economic analysis carried out for the power cycle. The changes in the latter table columns 2, 3, and 5, are with reference to dry steam cycle without corrosion mitigation. Using the presumptions stated in section 3.3, the overnight capital cost do change with enthalpy, as can be seen for the cases of $h = 2900 kJ/kg$ and $h = 3600 kJ/kg$. As does the cost per kW. The area of the heat exchanger used in the economic analysis was $23,000 m^2$ for the case of IDDP-1 but $22,000 m^2$ and $35,000 m^2$ for the cases with $h = 2900 kJ/kg$ and $h = 3600 kJ/kg$, respectively.

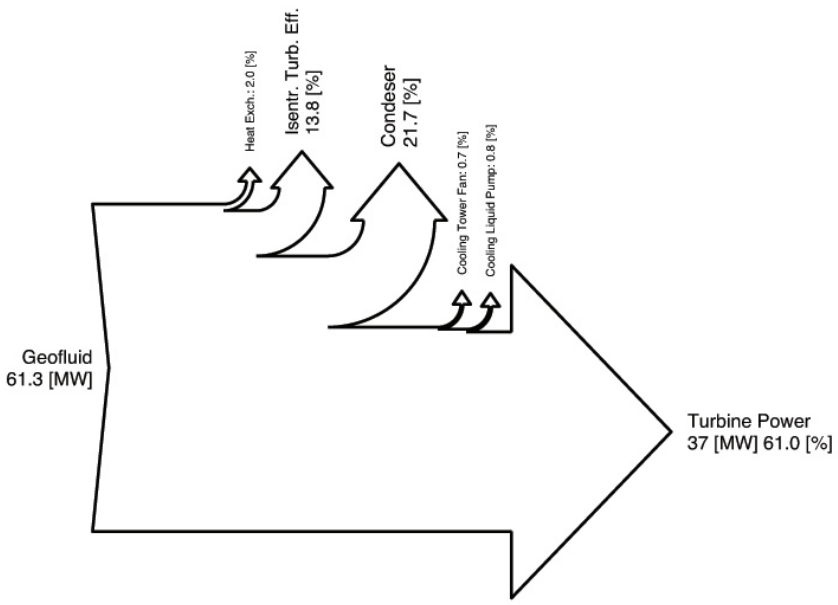

Figure 50: Results from exergy analysis for a binary cycle. The Grassmann diagram shows the amount of exergy lost in each process in the power cycle.

Table 10: Results from economic analysis of binary cycle

Case	Net Power [MW]	Cost of Corrosion Mitigation System [$\$ * 10^6$]	Overnight Capital Cost [$\$10^6$]	Monthly O$M Cost [$\$ * 10^3$]
IDDP-1	37.1	20	120	120
h=2900kJ/kg	47.7	20	140	160
h=3600kJ/kg	47.4	28	150	160

Table 11: Additional results from economic analysis of binary cycle

Case	Increase in Overnight Capital Cost [$\$ * 10^6$]	Change in Power [MW]	Cost per kW [$\$/kW$]	Increase in Cost per kW [$kW]
IDDP-1	17	-2.9	3200	700
h=2900kJ/kg	17	-2.3	3000	500
h=3600kJ/kg	25	-2.6	3200	700

5 Discussion

After analyzing each mitigation method in detail it is interesting to observe their power outputs in the same figure, for comparison. This way it can be determined what method is best for a given enthalpy and wellhead pressure. Future decision makers, dealing with corrosive boreholes, have the possibility of using the enthalpy of their borehole and the wellhead pressure, that gives the highest mass flow rate, and see what mitigation methods suit them best.

5.1 Comparison of the Mitigation Methods

5.1.1 Geofluid with Enthalpy of 2900kJ/kg

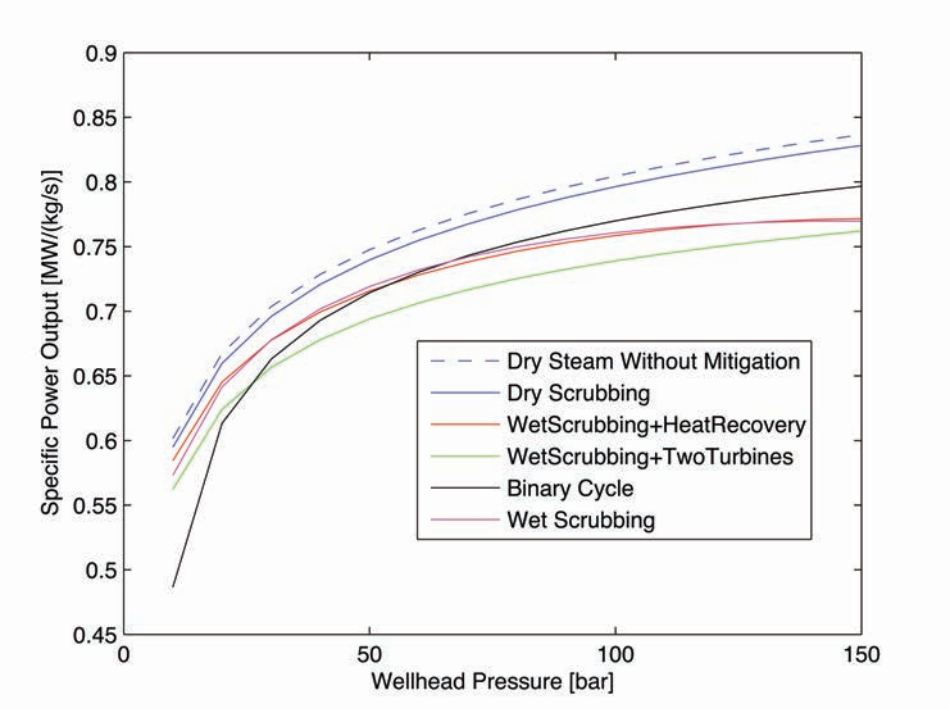

Figure 51: Specific net power output from each mitigation method. The figure shows which method gives the most power output for a given wellhead pressure. The power output is given for a geofluid with enthalpy at wellhead of 2900kJ/kg.

Figure 51 shows the specific net power output for all the mitigation methods. These are the same curves as shown in figures 22, 27, 47, 32, 37, and 42, only together this time.

Dry scrubbing gives the highest net power output at a given moment, as expected. At low wellhead pressures, the difference is smallest but increases with the pressure. This is of course because dry scrubbing offers the smallest destruction of superheat.

Wet scrubbing is similar to dry scrubbing at low pressures, but as the pressure increases, so does the difference. At high pressures the power output seems to have reached its asymptote, for all excess superheat gained by higher pressures is destroyed by injection of water preventing the net power output from increasing.

Wet scrubbing with heat recovery doesn't affect the net power output significantly. The power curve lies close to the one for wet scrubbing without heat recovery. The superheat of geofluid with enthalpy of 2900kJ/kg is so little that there is no essential conservation of superheat by adding the heat exchanger into the power cycle. The extra capital cost of the heat exchanger could not be justified for a geofluid with this enthalpy.

For wet scrubbing with an additional turbine it can be seen that as the pressure increases it gets more feasible with respect to the other methods. Maybe it would be a better choice at pressures higher than 150bar, as it has almost reached wet scrubbing and wet scrubbing with heat recovery. The extra capital cost of adding another turbine into the power cycle could not be justified for a geofluid with this enthalpy.

The binary cycle produces the lowest power at low pressures. At 30bar it exceeds the wet scrubbing with an additional turbine, and at $50-60$bar it exceeds both wet scrubbing and wet scrubbing with heat recovery.

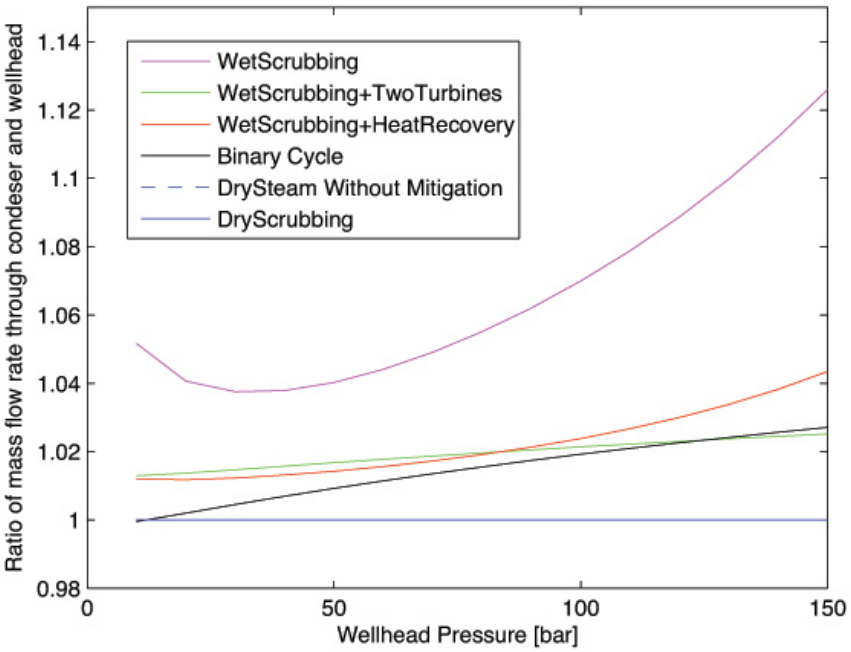

Figure 52: Ratio of mass flow rate of geofluid (working fluid) through condenser and the mass flow rate of geofluid (2900kJ/kg) at the wellhead,. Note that lines corresponding to direct use and dry scrubbing coincide, for there is no change in mass flow rate.

The ratio between the mass flow rate through the condenser and at the wellhead is proportional to the ratio of cooling requirement between corrosion mitigation methods. For example, 5% increase in mass flow rate through a condenser requires the same increase in cooling, requiring a larger cooling tower. Figure 52 shows that the traditional setup of wet scrubbing requires around 4-12% more cooling than the other mitigation methods.

5.1.2 Geofluid with Enthalpy of 3600 kJ/kg

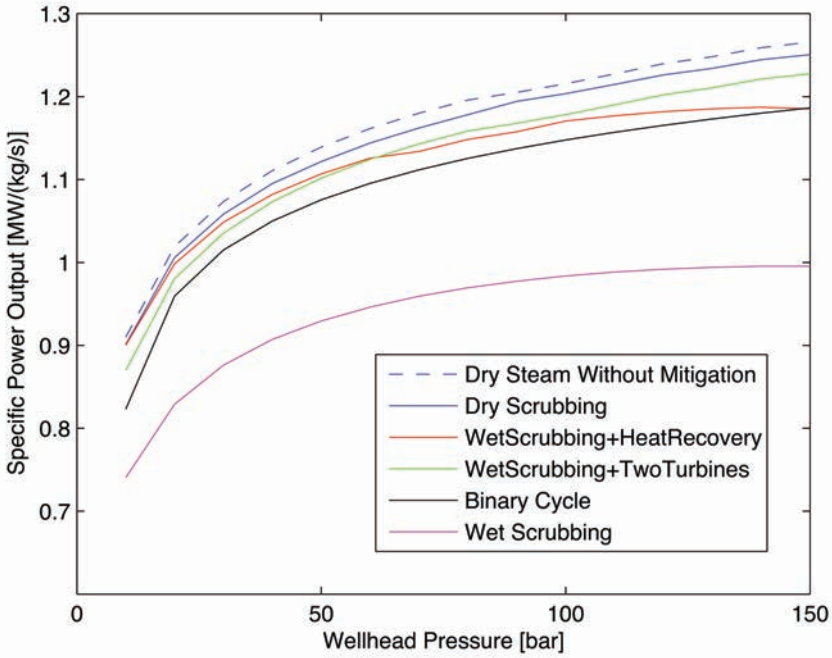

Figure 53: Specific net power output from each mitigation method. The figure shows which method gives the most power output for a given wellhead pressure. The power output is given for a geofluid with enthalpy at wellhead of 3600kJ/kg.

Figure 53 shows the specific net power output for all the mitigation methods. Again, these are the same curves as shown in figures 23, 28, 48, 33, 38, and 43, only together this time.

Dry scrubbing gives the highest power output out of the five mitigation methods, but at pressures of 10*bar* it is the same as wet scrubbing with heat recovery and wet scrubbing with an additional turbine.

Wet scrubbing has the lowest power output of all the mitigation methods. It gives around 16% less power than the other methods. The asymptote at this enthalpy seems to lie around 1MW/(kg/s).

Wet scrubbing with heat recovery is just as good as dry scrubbing at lower pressures. As the wellhead pressure increases, the method gets relatively worse. It is clear that when the geofluid

has a considerable amount of superheat, heat recovery system with traditional wet scrubbing can have a great affect on the power output of the cycle.

Wet scrubbing with an additional turbine is similar to dry scrubbing at all pressures. It is clear that an additional turbine in the power cycle makes for almost no losses, compared to direct use.

The binary cycle in this case produces more power than wet scrubbing at all pressures, but slightly less than the other methods. It can be seen that wet scrubbing with heat recovery collides with the binary cycle at 150*bar*, giving the sense that a binary cycle might be more appealing at higher pressures.

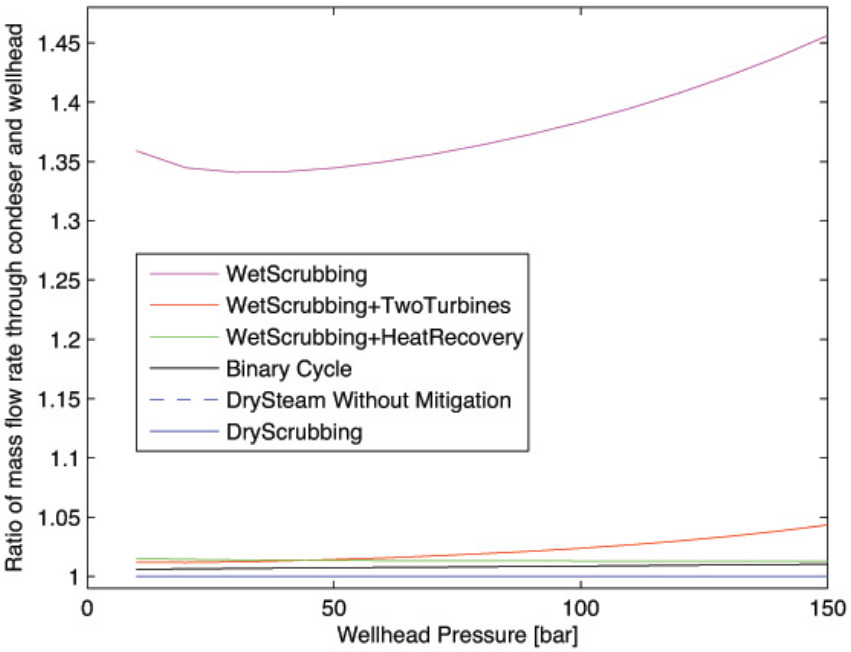

Figure 54: Ratio of mass flow rate of geofluid (working fluid) through condenser and the mass flow rate of geofluid (3600kJ/kg) at the wellhead. Note that lines corresponding to direct use and dry scrubbing coincide, for there is no change in mass flow rate.

In figure 54 it can be seen that as the enthalpy of the geofluid increases, so do the cooling requirements of the corrosion mitigation methods. The most significant increase is in the traditional setup of wet scrubbing, in this situation it requires around 35-45% more cooling than the other mitigation methods.

5.1.3 IDDP-1

Figure 55 shows the net power output for all the mitigation methods using the deliverable curve for IDDP-1 and enthalpy of 3100kJ/kg. Again, these are the same curves as shown in

figures 24, 29, 49, 34, 39, and 44, only together this time.

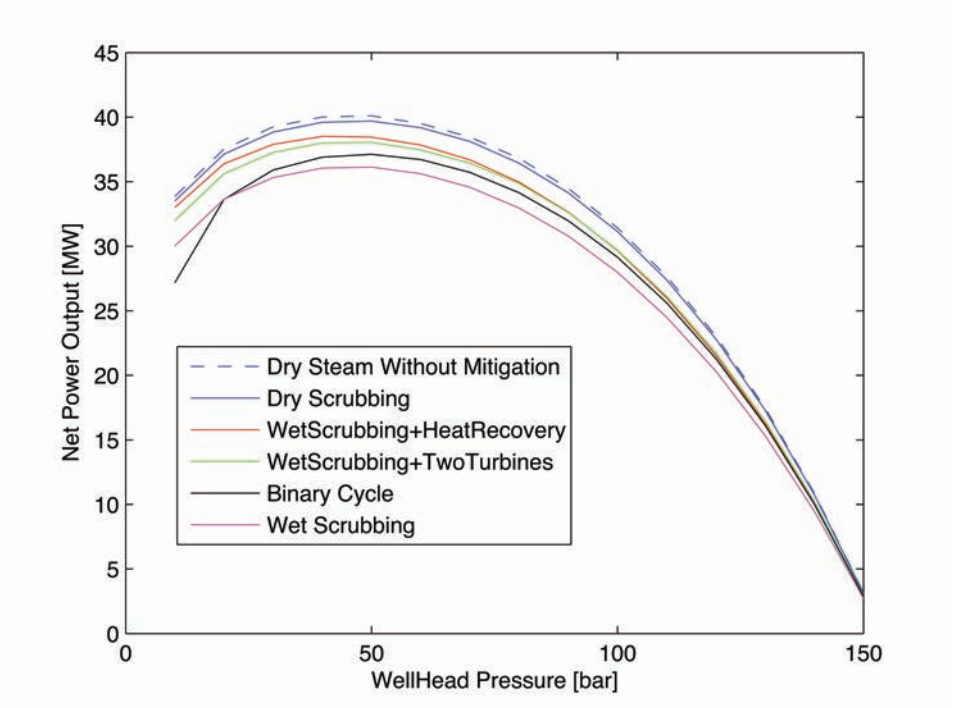

Figure 55: Net power output from each mitigation method using the deliverability curve for IDDP-1 and enthalpy of 3100kJ/kg. The figure shows which method gives the most power output for a given wellhead pressure.

It is clear that the optimum wellhead pressure lies between $40-50$bar. At those pressures, the power output of the mitigation methods differs by around 5MW. Figure 55 shows evidently the potential of IDDP, for the corrosion mitigation method with the lowest power output, still delivers power an order of magnitude higher than a conventional well [21].

Figure 56 shows that the traditional setup of wet scrubbing requires around 15% more cooling than the other mitigation methods.

It can be seen on the Grassmann diagrams shown in figures 25, 30, 35, 40, 45, and 50, that the dry steam cycle without corrosion mitigation has the least amount of losses due to the isentropic turbine efficiency. The reason is that the turbine in this power cycle has the highest degree of superheat at its inlet. Consequently, it has the biggest fraction of dry expansion of all the power cycles. This is supported by the fact that dry steam cycle with dry scrubbing has the second lowest losses due to the isentropic turbine efficiency.

It surprising to see how little exergy is lost in the wet scrubbing process. The losses are compensated by the increase in mass flow rate due to the injection liquid.

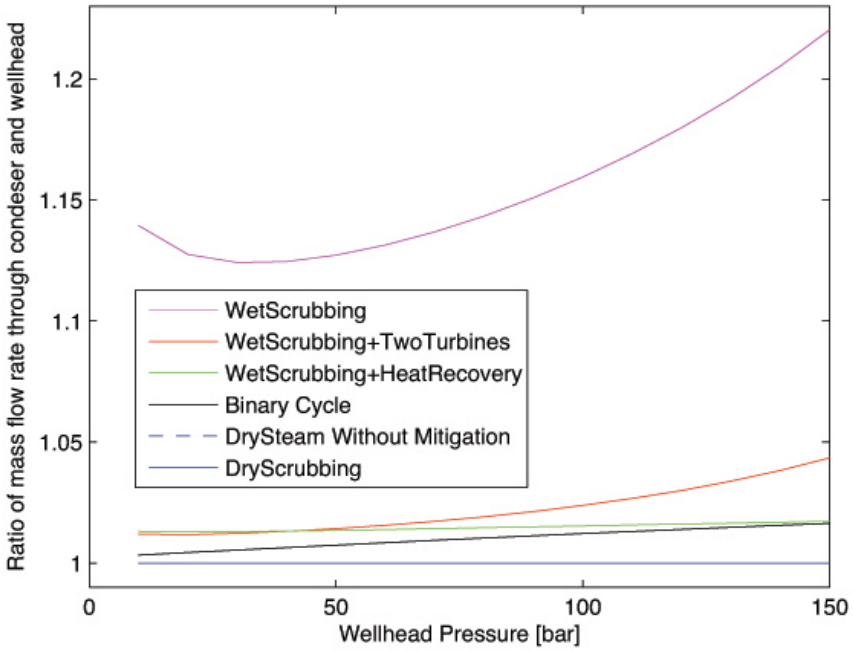

Figure 56: Ratio of mass flow rate of geofluid (working fluid) through condenser and the mass flow rate of geofluid at the wellhead. Note that lines corresponding to direct use and dry scrubbing coincide.

5.2 Selection of a Power Cycle for Geofluid with Enthalpy of 3600kJ/kg and Pressure of 10bar

Figure 21 shows the thermodynamic process that a geofluid with $h = 3600kJ/kg$ at $p = 10bar$ would undergo in a dry steam cycle without corrosion mitigation. Comparing this with Figure 36, it can be seen that the process that the geofluid undergoes does not change much between the two methods. It can be argued that if a well with such an enthalpy were to be exploited at low pressures, corrosion mitigation such as wet scrubbing might, in theory, not be needed. Dry steam cycle without corrosion mitigation, where the steam is not allowed to condense in the turbine, might give the best power output to cost ratio.

5.3 High utilization efficiency

Figures 22, 23, 24, 27, 28, 29, 32, 33, 34, 37, 38, 39, 42, 43, 44, 47, 48, and 49. show the utilization efficiency of the power cycles for different enthalpies. This high efficiency, ranging from 46-73%, may come as a surprise to the reader, but the reason for this is the high value of the incoming exergy. It has to be pointed out, however, that the first law efficiency (the efficiency of the energy conversion process as defined by the first law of thermodynamics, expressed as the net produced work, divided by the energy input) is around 20-35% for all power cycles.

5.4 Cost Analysis

The tables in this section compare the results from tables 1, 2, 3, 4, 5, 6, 7, 8, 9, 10, and 11.

5.4.1 Geofluid with Enthalpy of 2900kJ/kg

The capital and monthly operational and maintenance costs are shown in tables 12 and 13. A good and efficient implementation of dry steam scrubbing has the potential of increasing the power output by 1.4MW , with respect to wet scrubbing, but at the same time increasing the capital cost per kW produced and keeping similar O&M costs. At such a low enthalpy, wet scrubbing with Heat recovery, wet scrubbing with an additional turbine, and a binary cycle do all give lower power output than wet scrubbing for higher costs.

Table 12: Comparison of results from economic analysis on the different models for the case of enthalpy of 2900kJ/kg

Method	Power [MW]	Cost of Corrosion Mitigation System [$\$ * 10^6$]	Overnight Capital Cost [$\$10^6$]	Monthly O$M Cost [$\$ * 10^3$]
Direct Use	50.0	-	130	160
WS	48.1	0.20	120	170
WS with Heat Rec.	47.9	1.4	120	170
WS with an Add. Turb.	46.4	0.85	120	160
DSS	49.5	1.0	130	170
Binary cycle	47.7	20	140	160

Table 13: Additional comparison of results from economic analysis on the different models for the case of enthalpy of 2900kJ/kg

Method	Increase in Overnight Capital Cost [$\$ * 10^6$]	Change in Power [MW]	Cost per kW [$\$/kW$]	Increase in Cost per kW [$kW]
Direct Use	-	-	2500	-
WS	-1.7	-1.9	2600	100
WS with Heat Rec.	-0.76	-2.1	2600	100
WS with an Add Turb.	-2.8	-3.6	2600	100
DSS	0.46	-0.54	2500	0
Binary cycle	17	-2.3	3000	500

5.4.2 Geofluid with Enthalpy of 3600kJ/kg

The capital and monthly operational and maintenance costs are shown in tables 14 and 15. A good and efficient implementation of dry steam scrubbing has the potential of increasing the power output by 8.4MW , with respect to wet scrubbing, and at the same time lowering the capital cost per kW produced and O&M costs significantly. At these enthalpies, wet scrubbing with heat recovery seems to be a feasible alternative to wet scrubbing from an economic point of view. wet scrubbing with an additional turbine produces 7.5MW more than wet scrubbing, but the high capital costs tone down the feasibility of the method. Again, binary cycle does not seem to be a feasible option.

Table 14: Comparison of results from economic analysis on the different models for the case of enthalpy of 3600kJ/kg

Method	Power [MW]	Cost of Corrosion Mitigation System [$\$ * 10^6$]	Overnight Capital Cost [$\$10^6$]	Monthly O$M Cost [$\$ * 10^3$]
Direct Use	50.0	-	130	160
WS	40.7	0.20	120	150
WS with Heat Rec.	48.7	9.1	130	170
WS with an Add. Turb.	48.2	16	140	170
DSS	49.1	1.0	130	170
Binary cycle	47.4	28	150	160

Table 15: Additional comparison of results from economic analysis on the different models for the case of enthalpy of 3600kJ/kg

Method	Change in Overnight Capital Cost [$\$ * 10^6$]	Change in Power [MW]	Cost per kW [$\$/kW$]	Increase in Cost per kW [$kW]
Direct Use	-	-	2500	-
WS	-9.6	-9.3	2800	300
WS with Heat Rec.	7.7	-1.3	2700	200
WS with an Add Turb.	14	-1.8	2900	400
DSS	0.12	-0.88	2500	0
Binary cycle	25	-2.6	3200	700

5.4.3 IDDP-1

The capital and monthly operational and maintenance costs are shown in tables 16 and 17. It is obvious that dry steam scrubbing possesses much potential for improvement in corrosion mitigation systems. A good and efficient implementation of DSS has the potential of increasing the power output from IDDP-1 by 3.4MW , with respect to wet scrubbing, and simultaneously lowering capital cost per kW produced and keeping similar O&M costs. A binary cycle with a heat exchanger made out of titanium seems to be the most expensive corrosion mitigation.

Table 16: Comparison of results from economic analysis on the different models for the case of IDDP-1

Method	Net Power [MW]	Cost of Corrosion Mitigation System [$\$ * 10^6$]	Overnight Capital Cost [$\$ * 10^6$]	Monthly O$M Cost [$\$ * 10^3$]
Direct Use	39.4	-	99	130
WS	35.5	0.20	95	130
WS with Heat Rec.	37.7	4.3	100	140
WS with an Add. Turb.	37.3	5.8	100	130
DSS	38.9	1.0	99	130
Binary cycle	36.5	20	120	120

Table 17: Additional comparison of results from economic analysis on the different models for the case of IDDP-1

Method	Change in Overnight Capital Cost [$\$ * 10^6$]	Change in Power [MW]	Cost per kW [$\$/kW$]	Change in Cost per kW [$kW]
Direct Use	-	-	2500	-
WS	-3.9	-3.9	2700	200
WS with Heat Rec.	2.6	-1.7	2700	200
WS with an Add Turb.	3.6	-2.1	2700	200
DSS	0.50	-0.50	2500	0
Binary cycle	17	-2.9	3200	700

5.5 Benefits of Drilling Deeper

It is seems that deep drilling possesses potential for the geothermal industry, for the first borehole may be an order of magnitude more powerful than a traditional one. But as the development goes on, and enthalpy of accessible geofluids from new boreholes comes closer and closer to 3600kJ/kg, the development of scrubbing technologies to replace wet scrubbing becomes ever more important. It has been shown that a good and efficient implementation of dry steam scrubbing may increase the power output of a single borehole significantly.

6 Conclusion

As IDDP will get closer to its goals of even higher temperatures and enthalpy, the availability of other corrosion mitigation methods than wet scrubbing becomes more important. It has been shown that the destruction of superheat, caused by wet scrubbing at high enthalpies, may result in loss of considerate power. At low enthalpies and high wellhead pressures, wet scrubbing with an additional turbine does not seem to be a feasible option because of the low degree of superheat in the steam. On the other hand, at higher enthalpies, where the degree of superheat is very high, it may be uneconomic to use wet scrubbing and a second turbine step in the power cycle; the dry turbine expansion extracts most of the power anyway. A binary cycle seems to be more expensive than the other methods, regardless of enthalpy of the geofluid. It has been shown that dry steam scrubbing gives the highest power output for all enthalpies and wellhead pressures, and at the same time keeps the best $\$/kW$ ratio.

It is the destruction of superheat, rather than exergy, that causes wet scrubbing to produce less power with increasing enthalpy, with respect to the other methods examined. The increase in mass flow rate in the wet scrubbing minimizes the total loss of exergy in the stream, while the destruction of superheat decreases the efficiency in the turbine.

It is clear that the IDDP may possess potential for development in the geothermal industry. It has been shown that the first well, IDDP-1, is expected to produce around 8 times more power than a traditional borehole.

7 Future Work

In this study, six different implementations of power cycles with corrosion mitigation were analyzed and compared. It would be interesting to take parts of this study and examine them even further. Below are a few things that the author believes would be both interesting, and valuable to further development of corrosion mitigation in the geothermal sector.

There are many things to consider when constructing a steam-to-steam heat exchanger. Spotting the difficulties, examining them and overcoming, is essential for further development.

The cost of installing wet scrubbing and dry steam scrubbing has to be examined in more detail.

The value for capital cost, $\$2,500/\text{kW}$ used in the economic analysis should be reevaluated, for it has been estimated that IDDP-wells are more expansive to construct than traditional ones. However, since they may be around 8 times more powerful the cost per kW might be lower. This affects the total capital cost of the corresponding power plant. A better value than the one above, will give more conclusive economic analysis.

This economic analysis covered only one type of wet and dry steam scrubbing, that is, using one injection material. A more detailed analysis might include other chemicals.

The wellhead pressure for IDDP-1 is not selected solely with respect to the highest power output. Other chemicals than HCl may precipitate at certain pressures. This has to be analyzed in more detail and examined as to whether it supports the wellhead pressures suggested in this study.

More research on dry steam scrubbing is essential to get more conclusive results for the power cycle. The estimations made in this study, described above, are considered to give acceptable results, but more can be done to support them.

A more thorough chemical analysis on how different materials for dry steam scrubbing react with HCl, and what affect other gases in the stream may have on the reaction.

8 Bibliography

[1] A. Bejan, G. Tsatsaronis, M. J. Moran. *Thermal Design and Optimization*. New York, NY: John Wiley & Sons, 1996.

[2] D. W. Fisher, D. B. Jung. "Alternatives to Traditional Water Washing Used to Remove Impurities in superheated Geothermal Steam." *Geothermal Resources Council Transactions*, vol. 20, pp. 737-741, 1996.

[3] E. T. Eliasson, S. Thórhalsson, B. Steingrímsson. "Geothermal Power Plants," presented at Short Course on Geothermal Drilling, Resource Development and Power Plants, Santa Tecla, El Salvador, 2011.

[4] E. Viviani, A. Paglianti, F. Sabatelli, and B. Tarquini. "Abatement of Hydrogen Chloride in Geothermal Power Plants." *Proc. World Geothermal Congress*, 1995, pp. 2421-2426.

[5] Icelandic Deep Drilling Project. "About." Internet: http://iddp.is/about/ [March, 2011].

[6] Icelandic Deep Drilling Project. "News, IDDP-1 drilled into magma at 2104 m depth." Internet: http://iddp.is/2009/06/iddp-1-drilled-into-magma-at-2104-m-depth/, June, 2009 [March, 2011].

[7] Icelandic Deep Drilling Project. "News, IDDP-1 flow test." Internet: http://iddp.is/2010/07/336/, July, 2010 [March, 2011].

[8] J. P. Holman. *Heat Transfer*. Singapore: McGraw-Hill, 2010.

[9] J. W. Tester, E. M. Drake, M. J. Driscool, M. W. Golay, W. A. Peters. *Sustainable Energy: Choosing amongst options*. Cambridge, MA: The MIT Press, 2005.

[10] K. A. Meeker, J. R. Haizlip. "Factors Controlling pH and Optimum Corrosion Mitigation in Chloride-bearing Geothermal Steam at The Geysers." *Geothermal Resources Council Transactions*, vol. 14, pp. 1677-1684, 1990.

[11] K. Ingason. "Re: Lokaverkefni - Kostnaðarmat & Ráðstefna" Personal e-mail (Nov., 2011).

[12] Landsvirkjun. "IDDP-1 Flow Test in 2010." Report: LV-2011/036, 2011.

[13] M. E. Inman, R. M. Sharp, P. T. Wilson, G. A. Wright. "On-line corrosion monitoring in geothermal steam pipelines." *Geothermics*, vol. 27, pp. 167-182, 1998.

[14] M. J. Moran, H. N. Shapiro. *Fundamentals of Engineering Thermodynamics*. New York, NY: John Wiley and Sons Inc., 2009.

[15] O. Weres, C. Kendrick. "Corrosion by HCl in Dry Steam Wells Controlled using Potassium Carbonate without Destoying Superheat." *Geothermal Resources Council Transactions*, vol. 34, pp. 1097-1104, 2010.

[16] Orkustofnun. ”Jarðhiti, Jarðvarmavinnsla, Jarðvarmavirkjanir.” Internet: http://www.os.is/jardhiti/jardhitanotkun/jardvarmavirkjanir/ [Sept., 2011].

[17] P. Hirtz, C. Buck, R. Kunzman. "Current Techniques in Acid-Chloride Corrosion Control and Monitoring at The Geysers." *Proc. Sixteenth Workshop on Geothermal Reservoir Engineering*, 1991, pp. 83-95.

[18] P. Hirtz, J. Miller, E. Prabhu. ”Operational Results of a Dry-steam Resource Chloride Corrosion Mitigation System.” *Geothermal Resources Council Transactions*, vol. 14, pp. 1667-1675, 1990.

[19] P. Hirtz, M. L. Broaddus, D. L. Gallup. ”Dry Steam Scrubbing for Impurity Removal from Superheated Geothermal Steam.” *Geothermal Resources Council Transactions*, vol. 26, pp. 751-754, 2002.

[20] R. C. Moore, R. E. Mesmer, J. M. Simonson. ”Solubility of Potassium Carbonate in Water between 385 and 529K Measured Using the Synthetic Method.” *Jounal of Chemical & Engineering Data*, vol. 42, pp. 1079-1081, 1997.

[21] R. DiPippo. *Geothermal Power Plants: Principles, Applications, Case Studies and Environment Impact*. North Dartmouth, MA: Butterworth-Heinemann, 2008.

[22] S. Hólmgerisson, Á. Guðmundsson, B. Pálsson, H. Á. Bóasson, K. Ingason, S. Þórhallson. ”Drilling Operations of the First Iceland Deep Drilling Well (IDDP).” *Proc. World Geothermal Congress*, 2010, pp. 1-10.

[23] S. Kaiser, K. Weigl, Spiess-Knafl, C. Aichernig, A. Friedl. ”Modeling a Dry-Scrubbing Flue Gas Cleaning Process.” *Chemical Engineering and Processing*, vol. 39, pp. 425-432, 2000.

[24] United Nations Environment Programme. ”Energy Efficiency Guide for Industry in Asia, Cooling Towers.” Internet: http://www.energyefficiencyasia.org/docs/ee_modules/Chapter-Cooling%20Towers.pdf, 2006 [Nov. 2, 2011].

[25] W. W. Peng. *Fundamentals of Turbomachinery*. Hoboken, NJ, John Wiley & Sons, 2007.

[26] Y. A. Cengel, M. A. Boles. *Thermodynamics, An Engineering Approach*. Singapore: McGraw-Hill, 2006.